Photocatalytic performance of alkali metal doped graphitic carbon nitrides and Pd-alkali metal doped graphitic carbon nitride composites

Diamond and Related Materials, Volume 125, May 2022, Article number 109006

Maciej Fronczak, Emília Tálas, Zoltán Pászti, Gábor P. Szijjártó, Judith Mihály, András Tompos, Piotr Baranowski, Santosh Kr. Tiwari, Michał Bystrzejewski

DOI: 10.1016/j.diamond.2022.109006

Document Type: Article

Source Type: Journal

ISSN: 09259635

Original language: English

Publisher: Elsevier Ltd

Corresponding author: Maciej Fronczak

Accepted: March 30 2022

Available online: 2 April 2022, Version of Record: 6 April 2022

Photocatalytic Performance of Alkali Metal Doped Graphitic Carbon Nitrides and Pd-Alkali Metal Doped Graphitic Carbon Nitride Composites

Maciej Fronczak[1*], Emília Tálas[2], Zoltán Pászti[2], Gábor P. Szijjártó[2], Judith Mihály[2], András Tompos[2], Piotr Baranowski[3], Santosh Kr. Tiwari[3], Michał Bystrzejewski[3]

[1] Faculty of Process and Environmental Engineering, Lodz University of Technology, Wólczańska 213, 93005 Łódź, Poland

[2] Institute of Materials and Environmental Chemistry, Research Centre for Natural Sciences, Eötvös Loránd Research Network (ELKH), Magyar tudósok körútja 2, 1117 Budapest, Hungary

[3] Faculty of Chemistry, University of Warsaw, Pasteura 1, 02093 Warsaw, Poland

Corresponding Author

*(Maciej Fronczak) Tel. +48 504872726 E-mail: maciej.fronczak@p.lodz.pl

Author Contributions

The manuscript was written with the contributions of all authors. All authors have given approval for the final version of the manuscript.

KEYWORDS: graphitic carbon nitride, palladium, alkali dopants, hydrogen production, photodegradation

ABSTRACT:

Although there are several reports about the beneficial performance of metal doped graphitic carbon nitrides (g-C_3N_4) in various photocatalytic reactions, the effect of different alkali metal dopants has not been studied systematically. Series of undoped, Li-, Na- and K-doped samples was synthetized and used for the preparation of novel type of photocatalysts, composed of palladium nanoparticles supported on alkali metals-doped graphitic carbon nitride. Palladium loading was achieved via citrate reduction of palladium precursor in the presence of the carbon nitride material. Several physicochemical characterization methods such as attenuated total reflection infrared- (ATR-IR), diffuse reflectance UV-visible spectroscopy, high-resolution transmission microscopy (HRTEM), energy dispersive spectroscopy (EDS), X-ray photoelectron spectroscopy (XPS), X-ray powder diffraction (XRD), and thermogravimetric analysis (TGA) were used to get information about the morphology and composition of the novel composites. According to the optical characterization results, the band gap of g-C_3N_4 decreased upon Na- and K doping but increased after Li-doping. The palladium nanoparticles were distributed over the support and appeared in dispersed (undoped g-C_3N_4, Li-g-C_3N_4) or agglomerated (Na-g-C_3N_4, K-g-C_3N_4) form with individual particle size below 5 nm. The catalytic performance of these composite materials was tested in two processes: (i) photodegradation of methyl orange and (ii) hydrogen production from methanol. The Na- doping of graphitic carbon nitride was found to be a key issue to enhance hydrogen production. The carbon nitride matrix was found to be stable during the photocatalytic experiments, while the Pd component underwent certain changes during the photocatalytic reforming reaction of methanol. Our results indicated that the really acting metallic Pd cocatalyst was formed mainly *in situ*.

HIGHLIGHTS

- Novel palladium-containing composites of graphitic carbon nitride were synthesized
- Alkali metal-doping significantly changed the band gap of graphitic carbon nitrides
- The same preparation method led to different Pd composites at the different dopants
- Na-doping enhanced the hydrogen production over the composite photocatalyst

1. Introduction

In 1990 Liu and Cohen predicted the existence of ultra-hard carbon nitride [1]. Since that time, the research has been focused on the synthesis and studying the properties of carbon nitride materials. Mesoporous graphitic carbon nitride (g-C_3N_4) has been found to be a suitable metal-free catalyst for the Friedel Crafts reaction [2]. It turned out to behave as a multifunctional catalyst, either due to its electronic properties, its nucleophilic properties, or its ability to form H bonds [3]. Although, in recent years, several important properties of g-C_3N_4 had been established, its photocatalytic performance has been the most commonly studied and widely known feature [4–6]. Graphitic carbon nitride is a semiconductor with a band gap of 2.7-3.0 eV [7,8], which results in its yellow or yellow-orange color and absorption of electromagnetic radiation in the wavelength range between 410 and 460 nm (visible light). There are lots of reports showing its significant activity in hydrogen generation under irradiation by visible light [7,9–11]. The efficiency of hydrogen production from the photochemical reduction of water was improved by approximately one order of magnitude via creating a mesoporous structure of polymeric C_3N_4 [11]. In line with the results of bandgap calculations, g-C_3N_4 exhibited visible-light activity also for O_2 evolution from water containing 0.01 M silver nitrate, although the activity for O_2 evolution was an order of magnitude lower than that for H_2 evolution [9].

Besides water splitting, g-C_3N_4 showed significant activity in the photodegradation of dyes, *e.g.*, methyl orange [4,12,13], rhodamine B [14], or methylene blue [15]. The source of the effectiveness of g-C_3N_4 in photocatalysis is connected with the formation of highly reactive radicals in the water splitting process over this material [16].

There are two main possibilities to modify g-C_3N_4. Firstly, the material can be a component in composites with other semiconductors, e.g. TiO_2 [17,18], ZnO [13] Ag_2O [19], or metallic

nanoparticles (NPs), e.g. Pd NPs [20,21], or Pt NPs [22–24]. The formation of the composites is carried out in order to obtain materials with better photocatalytic activity in comparison to pristine g-C_3N_4. As an example, Wang et al. reported that fluctuant H_2 evolution activity of bare g-C_3N_4 was stabilized and enhanced by modification with a small amount of Pt [9]. Composites of palladium with unmodified g-C_3N_4 [20,21] have been applied for a recyclable heterogeneous catalyst for reduction of nitroarenes [25,26], Suzuki coupling reaction [27], electrooxidation of formic acid and methanol [28], photodegradation of bisphenol A [29], hydrogen storage [30–32] and hydrogen generation [30].

In the second approach, carbon nitride can be doped with other elements, e.g., alkaline metals [33–40], or with various transition metals such as Fe, Cu, W, Co [10,41–43]. In most cases, the metal cations are incorporated into the crystal lattice of g-C_3N_4 [38]. The potassium-doping element was suggested to exist in intercalated from in the space between the g-C_3N_4 layers [44] or built-in g-C_3N_4 lattices by the formation of K-N bonds during the polycondensation process [36]. The zinc-doping element was found to be coordinated with the g-C_3N_4 framework through metal–N bonds [45]. In the case of Cu-doped g-C_3N_4, Cu ions were suggested to be chemically attached to the heptazine units through coordination bonds [10]. Sodium was found to be coordinated into the C-N rings by the N bridge linking of the triazine units [34,35] or into the interstitial sites of in-planar g-C_3N_4 enlarging the interlayer spacing [33], or incorporated both in the interlayer spacing and in the nitride pores [37] depending on the preparation method. Non-metal doping has also been described [6,8,46].

Doping is a useful tool in order to tune the photocatalytic performance of g-C_3N_4 [6,47]. In general, doping of g-C_3N_4 was reported to have enhanced activity in various photocatalytic reactions. The Zn dopant enhanced the photocatalytic reforming of MeOH under visible irradiation

(l > 420 nm) compared to undoped g-C_3N_4 [45]. Co-doped g-C_3N_4 resulted in increased photocatalytic water splitting activity in the presence of a triethanolamine scarifying agent [48]. K-g-C_3N_4 and Ti-g-C_3N_4 showed excellent activity in the photocatalytic degradation of phenol [39] and in the photocatalytic degradation of Rhodamine B under visible light [49], respectively. Cu-g-C_3N_4 was a successful electrocatalyst in the hydrogen evolution reaction (HER) [10].

Although there are several reports about the performance of metal doped g-C_3N_4 in various photocatalytic reactions, a comparison of the effect of different alkali metal dopants on the photocatalytic H_2 formation remains an undiscovered area. Moreover, a combination of the two modification routes, compositing of doped g-C_3N_4 with metal nanoparticles, has scarcely been reported in the recent literature. Accordingly, in this work, the synthesis and characterization of palladium NPs/g-C_3N_4 composites, in which g-C_3N_4 is previously doped with lithium, sodium, or potassium, is described. Photocatalytic behavior of these new composites in two different reactions, *i.e.*, photodegradation of methyl orange and methanol photocatalytic reforming reaction for hydrogen generation ($CH_3OH + H_2O \rightarrow CO_2 + 3H_2$) are compared. We also attempted to explore some relationships between the structural characteristics of our new types of composites and their photocatalytic behavior. In order to realize the changes of the catalysts during operation, results of characterization of fresh and recovered samples are also compared.

2. Experimental section

2.1. Chemicals

Cyanamide (>98%, Sigma Aldrich), lithium chloride monohydrate (>99%, Sigma Aldrich), sodium chloride (>99.8%, Sigma Aldrich), potassium chloride (>99.8%, Sigma Aldrich), silver nitrate (>99%, Sigma Aldrich), palladium(II) chloride (>98%. Sigma Aldrich), L-ascorbic acid (>99%, Sigma Aldrich), sodium hydroxide (>99%, Avantor Performance Poland), methyl orange (>98%, Avantor Performance Poland), concentrated hydrochloric acid (38 wt.%, Chempur), methanol (>99 %, Molar Chem), absolute ethanol (100.0 %, AnalaR NORMAPUR, VWR), hydrofluoric acid (38-41%, Reanal) and nitric acid (65 wt.%, Molar Chem) were applied in the experiments.

Double distilled water (18 MΩ) was used for the preparation of methanol solution and for dilution. The gases (H_2, N_2, Ar) used in this work were Linde products with 5.0 purity. The special mixture of 5% H_2 in N_2 for calibration of GC was bought from Messer.

2.2. Synthesis of Undoped and Doped graphitic carbon nitride

Graphitic carbon nitride and alkali metal-doped graphitic carbon nitrides were synthesized via the method described in detail elsewhere [38,40]. In brief, 15.9 g of cyanamide was annealed at 550^{o}C for 3h (undoped g-C_3N_4). The doped materials were obtained via annealing of the mixture of cyanamide and appropriate metal chloride, i.e., LiCl, NaCl, or KCl. The amount of the salt was adjusted to obtain a mixture containing 60 wt% of LiCl or 50 wt% of NaCl or 40 wt% of KCl. Importantly, the content of inorganic addition corresponded to the content of pure metal (Na or K) at the level of ca. 20 wt%. In the case of Li, the content of metal was 6.9 wt%. The higher content of Li was not possible because of the stoichiometry of lithium chloride monohydrate (11.5 wt %) and its limited water solubility. The materials were named X-g-C_3N_4, where X is the doping metal.

All chemicals used were of the highest available purity. The conversion yields (ratio of the mass of product to the mass of cyanamide) were 46 % (g-C_3N_4), 49 % (Li-g-C_3N_4), 43 % (Na-g-C_3N_4), or 46 % (K-g-C_3N_4), respectively. Each of the as-obtained product was washed once with 0.1 M HCl (RT, 500 cm^3) and distilled water (40 ^oC, 500 cm^3, few repetitions) until the supernatant was free of chloride anions (a test with $AgNO_3$ 5 wt.% aqueous solution).

2.3. Synthesis of Palladium Nanoparticles/Graphitic Carbon Nitride composites

The composites of palladium NPs with graphitic carbon nitrides were synthesized using a method similar to the preparation of palladium on activated carbon [50]. 2.5 grams of graphitic carbon nitride was suspended in 30 cm^3 of distilled water. The suspension was heated to 80^{o}C in a water bath and continuously stirred with a magnetic stirrer. Next, 2.5 cm^3 of a solution of palladium chloride in 1 M HCl (100 $mg \cdot cm^{-3}$) was dropped, and the suspension was stirred for 15 min. Then, 1 cm^3 of 0.1 M L-ascorbic acid was added (reducing agent). The suspension, which was originally yellow, changed its color to dark grey. After 30 min of stirring, the pH of the suspension was adjusted to 8 with a 10 wt% aqueous solution of NaOH. Then, the as-obtained composites were filtrated, washed with distilled water, and dried in air at 120^{o}C overnight.

2.4. Physicochemical characterization

Diffuse reflectance UV-visible spectra of the samples were registered using a Jasco V-570 UV-VIS spectrophotometer equipped with NV-470 type integrating sphere. The data were collected between 800 and 200 nm wavelengths with a 100 $nm \cdot min^{-1}$ scan rate.

Attenuated total reflection infrared (ATR-IR) spectra were recorded by means of a Varian 2000 (Scimitar Series) FT-IR spectrometer (Varian Inc, US) equipped with an MCT (Mercury-Cadmium-Telluride) detector and with a ‘Golden Gate’ diamond single reflection ATR unit

(Specac Ltd, UK). Sixty-four scans were collected at a spectral resolution of 4 cm^{-1}. Baseline correction was performed using the GRAMS/AI (7.02) software (ThermoGalactic Inc., US).

The transmission electron microscopy (TEM) images and high-resolution TEM images (HRTEM) were acquired using a Talos F200X microscope equipped with the field-emission X-FEG cathode. The microscope was combined with a Super X EDS detector. The limit of the resolution of the TEM microscope could be as low as 0.12 nm. The samples were also conducted to a mapping of each element in the studied samples.

TGA analyses were performed with the TA Q50 instrument under the atmosphere of oxygen and nitrogen (5 vol.% O_2) with the feeding rate of 65 $ml \cdot min^{-1}$ in the temperature range up to 900ºC.

The Pd and alkali content of the samples was measured by inductively coupled plasma-optical emission spectrometry (ICP-OES) technique by use of a simultaneous SPECTRO GENESIS instrument with axial plasma observation. Samples were measured after microwave-assisted dissolution in 1:2:6 mixtures of concentrated hydrofluoric acid: hydrochloric acid: nitric acid.

X-ray photoelectron spectroscopy (XPS) measurements were carried out using an EA125 electron spectrometer manufactured by Omicron Nanotechnology GmbH (Germany). The photoelectrons were excited by non-monochromatized MgKα (1253.6 eV) radiation. The spectra were recorded in the Constant Analyser Energy mode of the EA125 energy analyzer with 30 eV pass energy resulting in a spectral resolution of ca. 1 eV. The catalyst powders were suspended in isopropanol, and drops of the suspension were dried on stainless steel sample plates. Essentially in all cases, some charge-buildup was observed during the photoelectron spectroscopy measurement. Thus, the calibration of the binding energy scale was necessary. The main component of the N 1s spectrum attributed to the C-N=C bonding environment with a binding energy value of 398.6 eV [40,51–54] was selected as the reference point. With this charge

referencing, the main component of the C 1s spectrum (arising from the same C-N-C environments) appeared consistently around 288 eV, which is in good agreement with the literature data [40,51–54]. The collected data were processed using the CasaXPS software package by fitting the spectra with Gaussian-Lorentzian product peaks after removing a Shirley or linear background. Nominal surface compositions were calculated using the XPS MultiQuant software package [55] with the assumption of homogeneous depth distribution for all components.

X-ray powder diffraction (XRD) patterns were obtained in a Bruker D8 diffractometer using a Cu Kα radiation (1.54Å) in a 2θ angle range between 10 and 70. The materials were placed on the polymeric holder and flattened.

2.5. Photocatalytic characterization

2.5.1. Photodegradation of methyl orange

The process of photocatalytic degradation of methyl orange was conducted in a reactor of our own construction. The scheme of this reactor is presented in Figure S1 (Supplementary Data). The reactor was composed of a cylindrical glass vessel equipped with a water-cooled outer jacket. The inner space was filled with 300 cm^3 of methyl orange aqueous solution (10 $mg \cdot dm^{-3}$) with suspended 1.00 g of the studied sample. The reaction was carried out under continuous irradiation originated from a halogen lamp (500 W). The suspension was also continuously mixed with air bubbling. The process lasted 6 hours. The samples (1.5 cm^3) of the reaction mixture were taken every 30 minutes and were stored in the dark. The concentration of methyl orange was determined using a spectrophotometer (Shimadzu 2401-PC).

2.5.2. Photocatalytic hydrogen generation

In order to get information about the behavior of the undoped- and the alkali doped catalyst samples in photocatalytic methanol reforming, different experimental setups corresponding to different irradiation sources were used (see Figure S2 in the Supplementary Data). In the case of UV-visible light irradiation, a cylindrical quartz reaction vessel (140 mm in height and 60 mm in diameter) equipped with a magnetic stirrer, with a gas input and output, was used (Reactor UV). The light source was an Osram HQL de luxe lamp (125W) in a top irradiation arrangement. The reaction volume was 260 cm^3. The reaction under visible light irradiation was carried out in a Peschl Consulting type of photoreactor equipped with a gas input-output and with a homemade LED light source operated at four distinct wavelengths (400, 420, 440, 450 nm) (Reactor VIS). Due to the overheating of the LED series, the reaction time was limited to 60-100 minutes, and the irradiation was started at the highest wavelength in the Reactor VIS. The LED light source was immersed into a cooled quartz cylinder equipped with a stirrer, which provided higher light utilization than the top irradiation. The reaction volume was 330 cm^3 in Reactor VIS.

The concentration of the dispersed photocatalyst (0.5 $g \cdot dm^{-3}$) in both reactors was at the beginning of maximum photon absorption/the plateau region [56]. The initial concentration of methanol was 6 vol.% in distilled water, and the reaction was carried out at room temperature in every measurement. The two reactors were connected to a common analytical system (see Figure S2 in the Supplementary Data). Nitrogen gas with a 20 $cm^3 \cdot min^{-1}$ flow rate was continuously bubbled through the reactors. A gas chromatograph (Agilent 7820A) equipped with SUPELCO Carboxen 1010 column and TCD detector was used to follow the hydrogen production. The internal standard for GC analysis was argon gas added to the vapor-gas mixture before the GC sampling valve. The reaction effectiveness was expressed as hydrogen production rate ($mmol \cdot h^{-1}$).

According to the blank experiments, hydrogen formation was not observed without irradiation. The samples were recovered from the aqueous methanol solution by decantation and centrifugation after the photocatalytic reaction. They were washed with 3x50 cm^3 of absolute ethanol followed by drying under N_2 flow.

3. Results and discussion

3.1. Physicochemical characterization of g-C_3N_4 samples and Pd/g-C_3N_4 composites

In Figure 1. the results of diffuse-reflectance UV-Vis spectroscopic measurements over the different Pd-free, alkali metal doped g-C_3N_4 -s and the undoped sample are compared. It can be seen that the presence of Na (line a in Figure 1) and K (line b in Figure 1) dopant increased the absorbance and shifted the band edge to the visible range. However, the introduction of Li (line d in Figure 1) dopant decreased the absorbance and shifted the band edge to the UV range. The latter finding is in good agreement with the recent results in work by Jasni et al. [57].

As we have shown in our previous paper [38], the synthesis of Li-g-C_3N_4 via polycondensation of cyanamide in the presence of LiCl resulted in the presence of LiCl crystals in the obtained graphitic carbon nitride. For the other cases (i.e. NaCl, KCl), the metal ions were introduced without the chlorine anions. Thus, we assume that the presence of the chlorine ions significantly increased the band gap in comparison to the pure, non-doped g-C_3N_4.

Doping with sodium and potassium causes the tuning of the valence band and the conduction band. As shown in paper [24], alkali metals ions are coordinated between the heptazine rings, and the interaction of the graphitic carbon nitride with these ions decreases the band gap. The possible reason why the sodium doped sample exhibits the lowest band gap value is the consequence of that the sodium cation is smaller in comparison to the potassium ion. The size of the Na^+ ion does

not affect the crystal structure of the material as much as the larger K^+ ion. A similar conclusion has been presented in other work [39].

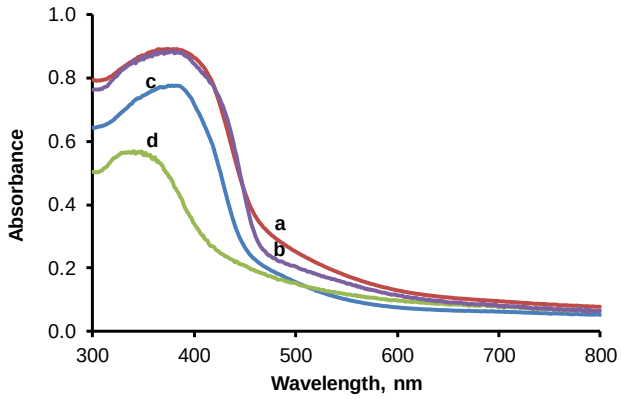

Figure 1. Diffuse-reflectance UV-Vis spectra of Pd-free Na-doped (a), K-doped (b), undoped (c), Li-doped (d) g-C_3N_4 samples

Table 1 contains the band gap values determined using the Tauc plot method [58–61]. In brief, the diffuse-reflectance UV-Vis spectra were transferred to the Tauc plots (Figures S3-S10), i.e., the curves which show the relation between the energy of the light and the quantity $(\alpha h\nu)^{1/2}$, where α is the absorption coefficient of the material. The band gap of the Pd-containing composites is lower in comparison to that of the graphitic carbon nitride supports in three cases (g-C_3N_4, Li-g-C_3N_4, and K-g-C_3N_4). In the case of sodium-doped material, the band gap is on the same level. Thus, the construction of composites primarily resulted in decreasing the band gap. This behavior is connected with the formation of the metal-semiconductor junction [62].

As seen in Table 1, Li doping increased the band gap, which confirms the results reported by Jasni et al. [57], while Na and K doping decreased that compared to the undoped g-C_3N_4 in line with literature data [24,33,36] Based on the results of XRD, HR-TEM, FT-IR, TGA, PL measurements, Jasni and et al. [57] concluded that Li atoms substitute the H atoms of the amino

groups. They assumed that the presence of Li^+ ions might lead to the formation of g-C_3N_4 with a small polymerization degree and more defect sites. They concluded from the data of UV-Vis analysis that Li^+ doping reduced the visible light sensitivity of the Li/g-C_3N_4 nanocomposites compared to g- C_3N_4 due to the distortion of the g- C_3N_4 planar structure. In order to interpret the effect of Na dopant, Liang et al. [24] determined VB by XPS measurements. They examined the effect of Na^+ doping on the relative position of CB and VB. Their results showed that Na^+ doping could down-shift the CB and VB edges of the g- C_3N_4 catalyst and decrease the band gap energy.

While the metal (palladium) and the semiconductor (graphitic carbon nitride) are contacted, electrons from the conduction band of the semiconductor transfer into the metal until the equilibrium of both Fermi levels are reached. This phenomenon causes the formation of an electron depletion region in the semiconductor, consisting of fixed cations. The resultant negative field lowers the band edges of the semiconductor in bulk in comparison to the energy at the interface. [63]. Most probably, the Fermi levels of palladium NPs and Na-g-C_3N_4 have similar values, and the changes in electronic structure are not significantly changed.

Table 1. Determined band gaps (E_g) of the materials obtained.

Material	Pure material		Composite with Pd NPs	
	E_g (eV)	λ_{MAX} (nm)	E_g (eV)	λ_{MAX} (nm)
g-C_3N_4	2.96	419	2.78	446
Li-g-C_3N_4	3.03	409	2.99	415
Na-g-C_3N_4	2.69	461	2.69	461
K-g-C_3N_4	2.75	451	2.70	459

ATR-IR spectra of Pd-free, alkali metal doped- and undoped g-C_3N_4 samples are shown in Figure 2. The spectrum of Pd-free g-C_3N_4 showed typical features in line with the literature [64]. The bands from 3300 to 3000 cm^{-1} were related to the stretching vibrations of N-H bonds due to the incomplete condensation of amino groups. The sharp bands at 806 and 889 cm^{-1} were assigned to the characteristic breathing mode of tri-s-triazine units and the deformation mode of N-H bonds, respectively. The bands between 1700-1200 cm^{-1} belong to stretching modes of CN heterocycles. The undefined band at 2180 cm^{-1}, despite the strong absorption of the diamond ATR crystal, referred to the presence of azide moiety [65]. The spectrum of Na- and K-doped samples was similar to that of g-C_3N_4. It seems plausible that the structure of g-C_3N_4 remained intact upon Na- and K-doping. The Li-doped sample, however, resulted in a different spectral feature. The high wavenumber bands corresponding to N-H stretching, as well as the disappearance of the sharp band at 889 cm^{-1}, suggested that the amino groups might participate in Li – g-C_3N_4 interaction. Jasni et al. characterized Li-modified g-C_3N_4 and revealed the substitution of H atoms of the amino groups by Li atoms [57]. They presumed that the presence of Li^+ ions enhanced the defect sites which in turn implies the distortion of the g-C_3N_4 planar structure. The splitting of the band around 1620 cm^{-1} and the significant shift in the wavenumbers of C-N and C=N related stretching bands were observed. In agreement with Jasni et al. [57], we suggested that the structure of g-C_3N_4 may be altered. Indeed, the bands at 1223 and 1195 cm^{-1} might belong to out-of-plane bending of the heptazine ring, which suggests that the planarity of the g-C_3N_4 sheets might have been altered. It is interesting to note that the triazine unit remained intact, as reflected by the band at 803 cm^{-1} assigned to the breathing mode of C_3N_4 subunits. The new band at 640 cm^{-1} was also observed by transient IR spectroscopy of Pt – g-C_3N_4 samples [66].

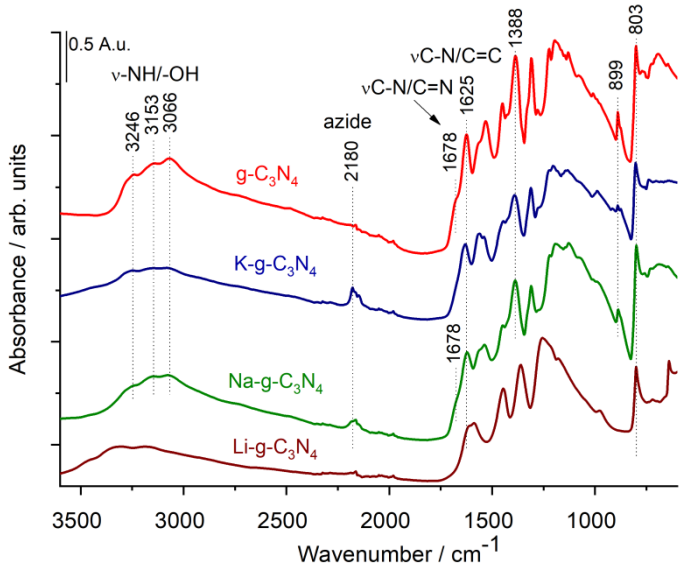

Figure 2. ATR-IR spectra of Pd-free, alkali metal doped and undoped g-C_3N_4 samples

In our previous paper [38], we showed that the dopant phase is mostly possibly present within the heptazine rings. We have shown the FTIR spectra, which undoubtedly proves this observation. The bands characteristic for the heptazine units are shifted comparing the doped samples and undoped samples. We assume that the dopant interacts by the coordinative bonds. The heptazine units comprise lone electron pairs onto the nitrogen atoms. This negatively charged spot is able to coordinate the positively charged metal cation.

From the above results, it could be seen that the spectroscopic and electronic features of the Na and K doped samples were similar, but the Li doped sample showed a significant difference. It is worth noting that according to the previous publication, the Li-doped sample had different morphology compared to the non-doped, K- and Na-doped g-C_3N_4 [38]. The lithium-doped g-C_3N_4 had the most developed porosity and the highest specific surface area (237.0 $m^2 \cdot g^{-1}$), whilst other samples had much lower surface area, namely 19.0 $m^2 \cdot g^{-1}$ for undoped, 0.8 $m^2 \cdot g^{-1}$ for Na doped, and 7.3 $m^2 \cdot g^{-1}$ for K doped g-C_3N_4, respectively [38]. The increased surface area, which is a

consequence of developed porosity possibly is a result of the rinsing of the lithium chloride small grains after the synthesis. These grains played the role of the soft template formed with molten lithium chloride. The melting point of LiCl is 605°C, which is close to 550°C, the constant temperature during synthesis. The overheating could occur as the result of the construction of the furnace and its relatively high inertness.

The TGA analysis at oxidizing atmosphere (Figure 3) and ICP-OES (Table 2) measurements were carried out to determine the content of palladium in the Pd/g-C_3N_4 composites. The g-C_3N_4 burns out at a higher temperature, and the as-formed gaseous products can be evacuated from the TGA crucible [7]. The thermal decomposition of the doped g-C_3N_4 (Li, Na, K) results in the formation of corresponding oxides (Li_2O, Na_2O, K_2O). The Pd-containing composites contain a mixture of the mentioned metal oxides and metallic palladium (palladium oxide decomposes above 750^{o}C [67]). The solid residue (its mass can be determined from the plateau of the TGA curve) is an indicator of the content of alkali metal dopant and as well the content of palladium. The content of palladium can be calculated as the difference between the percentage residue of the composite and the doped or undoped carbon nitride. It follows from TGA curves (Figure 3) that the content of palladium measured by this method varied between 4.1 and 9.4 wt%. The highest content was observed for Pd/Li-g-C_3N_4 composite. For the other cases, the Pd content was very similar, i.e., 4.1 wt.% (Pd/g-C_3N_4), 5.4 wt.% (Pd/Na-g-C_3N_4), and 4.9 wt.% (Pd/K-g-C_3N_4). The observed difference was plausibly connected with various specific surface areas presented in our previous paper [38]. As it is mentioned, Li-doped sample has much porous structure and strongly differs from the other three samples. When a big difference in the density of the samples exist, the volumes over the samples may be different in crucibles, and the possibility of complete burning is different, leading to the artifact. Furthermore, the putative stoichiometry for alkali oxide formation may be

disturbed by the different rates of peroxide formation/decomposition and the catalytic effect of Pd in case of the different doping elements.

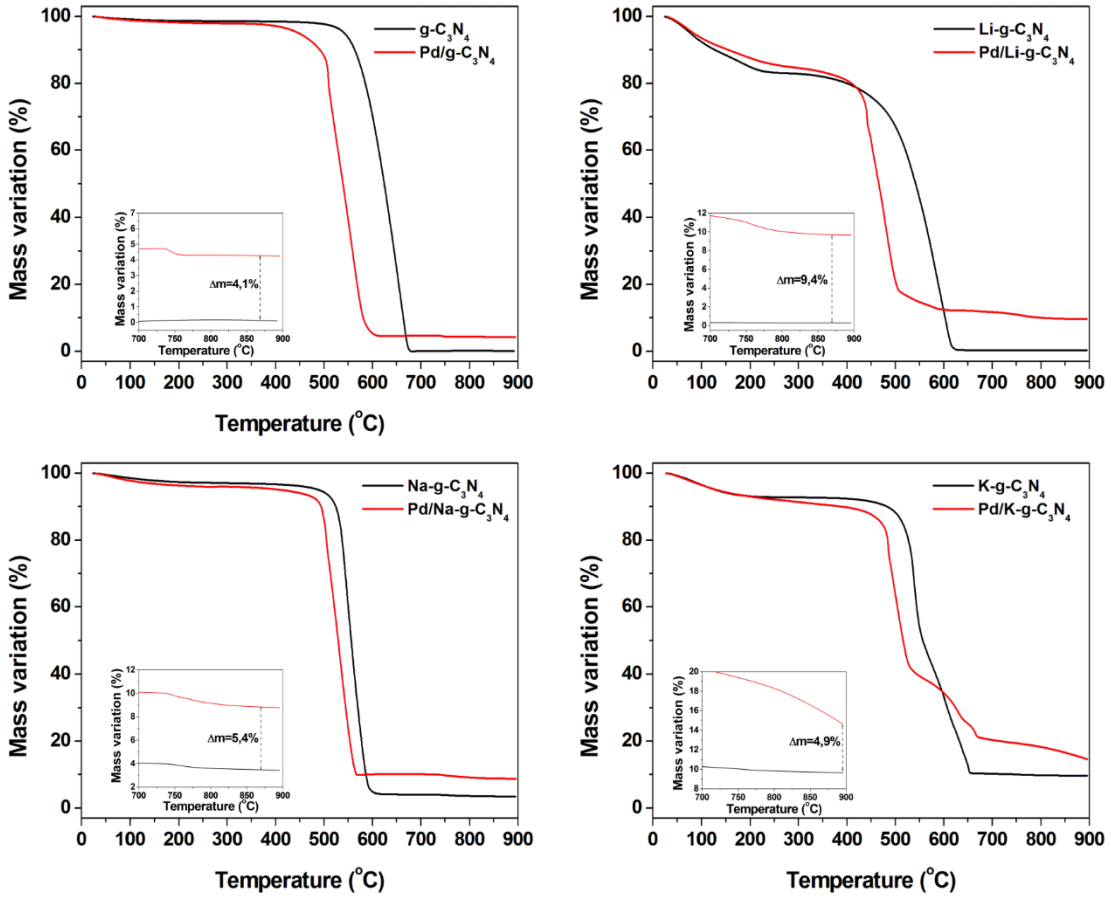

Figure 3. TGA curves of the materials determined under oxidizing atmosphere.

Alkali metal content of fresh and recovered Pd containing samples was measured by the ICP-OES technique (Table 2). The Li content of fresh Pd/Li-g-C_3N_4 was one order of magnitude lower than the Na and K content of the corresponding samples. This observation is in line with the assumed way of formation of high pore volume in the case of Li-g-C_3N_4. Na content was almost stable, but Li and K content decreased significantly during the reaction, which may indicate the different positions of the different dopants and their different interactions with the g-C_3N_4 matrix. It seems surprising that Na appeared in the other doped samples. A possible explanation is that the

rather high number of basic surface groups (and higher point of zero charge) of the Pd free Li-g-C_3N_4 and K-g-C_3N_4 [38] coordinate the Na^+ ions to the surface during the Pd loading.

Table 2. Metal contents of the fresh composites (with comparison to contents estimated from TGA data) and the samples recovered after the H_2 evolution reaction measured by ICP-OES

Catalyst	ICP-OES[a]					TGA
	dopant, wt.%		Pd, wt.%			Pd, wt.%
	Fresh	Recovered[b]	Fresh	Recovered[b]	Recovered[c]	Fresh
Pd/g-C_3N_4	none	none	3.4	3.4	3.6	4.1
Pd/Li-g-C_3N_4	0.29	0.03	4.0	2.1	2.4	9.4
Pd/Na-g-C_3N_4	4.66	4.29	4.7	4.9	4.8	5.4
Pd/K-g-C_3N_4	4.17	2.67	4.2	2.7	2.8	4.9

[a]average of 3 parallel measurements [b]recovered from Reactor UV [c]recovered from Reactor VIS

A comparison of the fresh and the recovered samples shows that various effects were observed for the different doping metals. According to the ICP-OES data, the bulk Pd content of Pd/g-C_3N_4 and Pd/Na-g-C_3N_4 samples did not change significantly during the photocatalytic reaction. The XPS analysis showed that the surface palladium concentration of Pd/g-C_3N_4 remained unchanged during the tests. However, the surface palladium concentration of Pd/Na-C_3N_4 decreased. Based on these observations, it can be concluded that sintering or a certain type of aggregation of Pd nanoparticles appeared in this sample. On the contrary, ICP-OES data revealed a decrease in bulk Pd content for Pd/Li-g-C_3N_4 and Pd/K-g-C_3N_4 samples during the photocatalytic reaction. It is obvious that the surface Pd concentration also decreased. If we accept that the rather high number of basic surface groups (and much higher point of zero charge) in Li-g-C_3N_4 and K-g-C_3N_4 samples coordinated the Na^+ ions to the surface in the company of counterions, it means a very different electrical environment which may result in a different binding force for the Pd nanoparticles on the surface compared to the other two samples. Consequently, the possibility of mechanical abrasion via the intensive mechanical stirring during the photocatalytic reaction is higher in the

case of Pd/Li-g-C_3N_4 and Pd/K-g-C_3N_4 samples, than in case of Pd/g-C_3N_4 and Pd/Na-g-C_3N_4 samples.

The morphology of the fresh composites was examined via TEM, and representative micrographs are presented in Figure 4. In the case of Pd/g-C_3N_4 (Figure 4a) and Pd/Li-g-C_3N_4 (Figure 4b), the palladium exists in the form of NPs of size below 5 nm. Sun et al. [27] synthesized the Pd/g-C_3N_4 composite with similar content of Pd. The size of Pd particles was found to be lower than 5 nm, thus similar to our findings. A similar size of obtained palladium NPs was also obtained by Zhao et al. [26]. For two other materials, i.e., Pd/Na-g-C_3N_4 (Figure 4 c, d) and Pd/K-g-C_3N_4 (Figure 4 f), the NPs (also their size is below 5 nm) are connected and form agglomerates. The size of the agglomerates is in the range of 20-100 nm. Importantly, the observed agglomerates are very regular in shape. The probable reason for the aggregate formation on Na- and K-g-C_3N_4 was the extremely small specific surface area of these graphitic carbon nitrides (0.8 $m^2 \cdot g^{-1}$, 7.3 $m^2 \cdot g^{-1}$ for Na- and K-doped samples, respectively) [38].

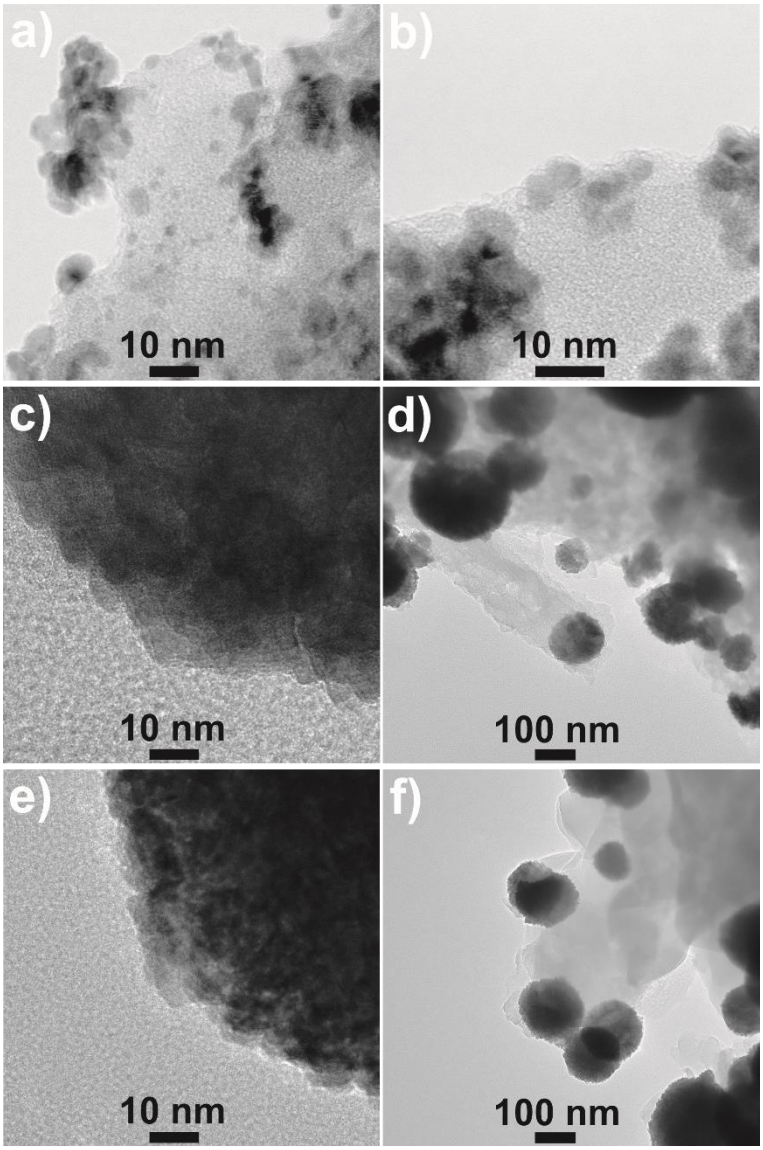

Figure 4. TEM images of a) Pd/g-C_3N_4, b) Pd/Li-g-C_3N_4, c),d) Pd/Na-g-C_3N_4, e), f) Pd/K-g-C_3N_4.

Additionally, the studied composites were mapped using EDS. Figures 5-8 present the distribution maps of palladium, carbon, nitrogen, doping element (excl. lithium), and oxygen. The mapping of lithium was impossible due to the absence of a special detector. Importantly, the positions of carbon and nitrogen in each sample are almost identical, and this is proof of the

presence of a carbon nitride matrix. The presence of oxygen originates from the partial oxidation of the samples and is in good agreement with our previous reports [38,40], where each material obtained exhibits oxidation of the surface. The distribution of Pd in each sample is irregular, whilst for the cases of other elements, their distribution is regular in the whole material.

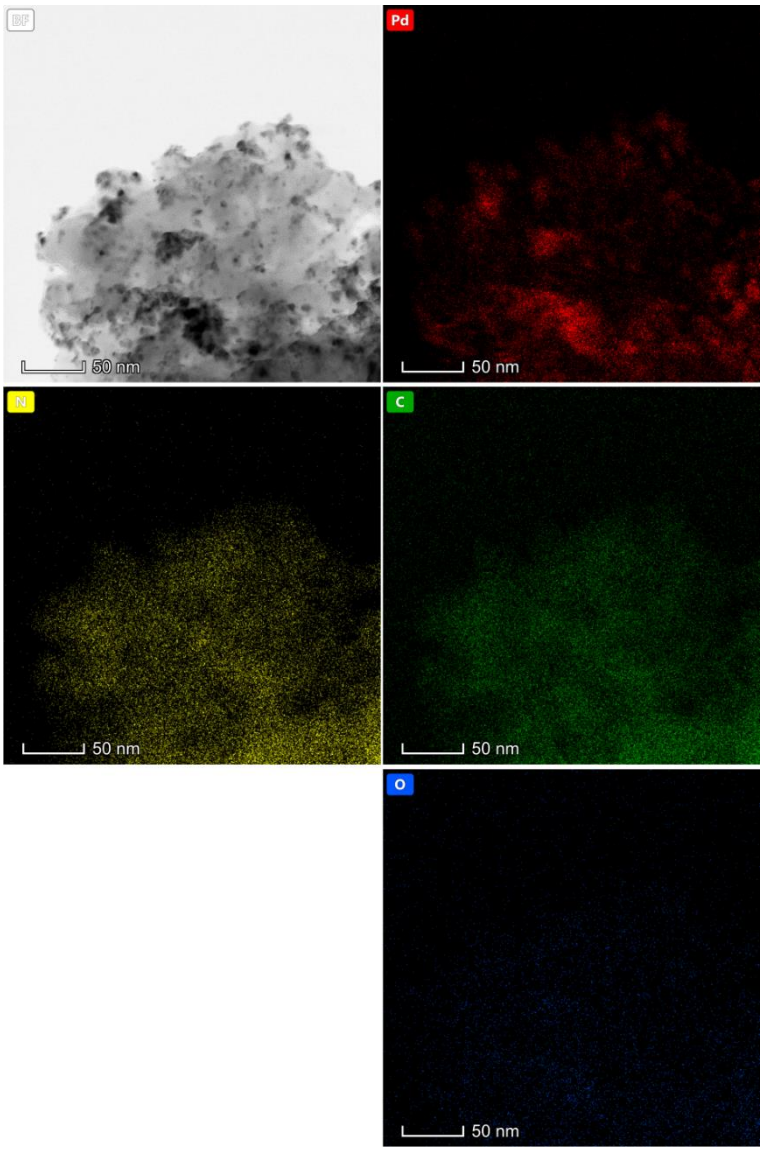

Figure 5. TEM image of the Pd/g-C_3N_4 composite and distribution of palladium, carbon, nitrogen, and oxygen (in false colors).

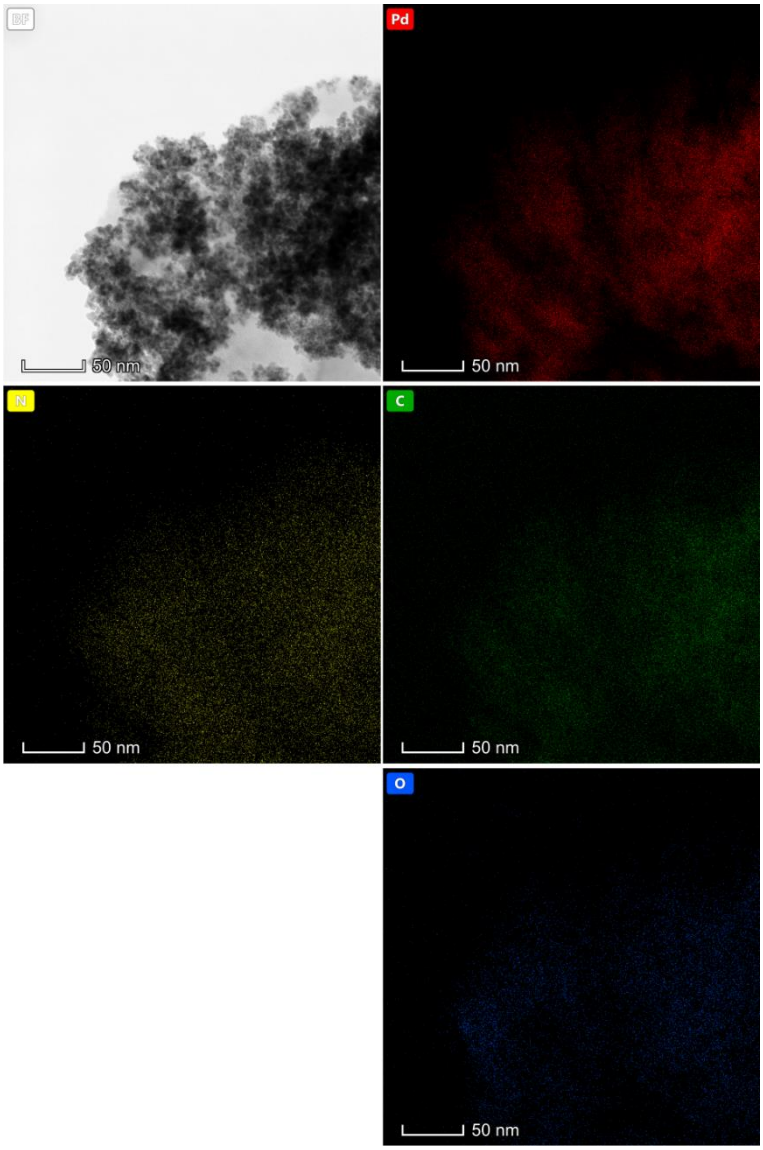

Figure 6. TEM image of the Pd/Li-g-C_3N_4 composite and distribution of palladium, carbon, nitrogen, and oxygen (in false colors).

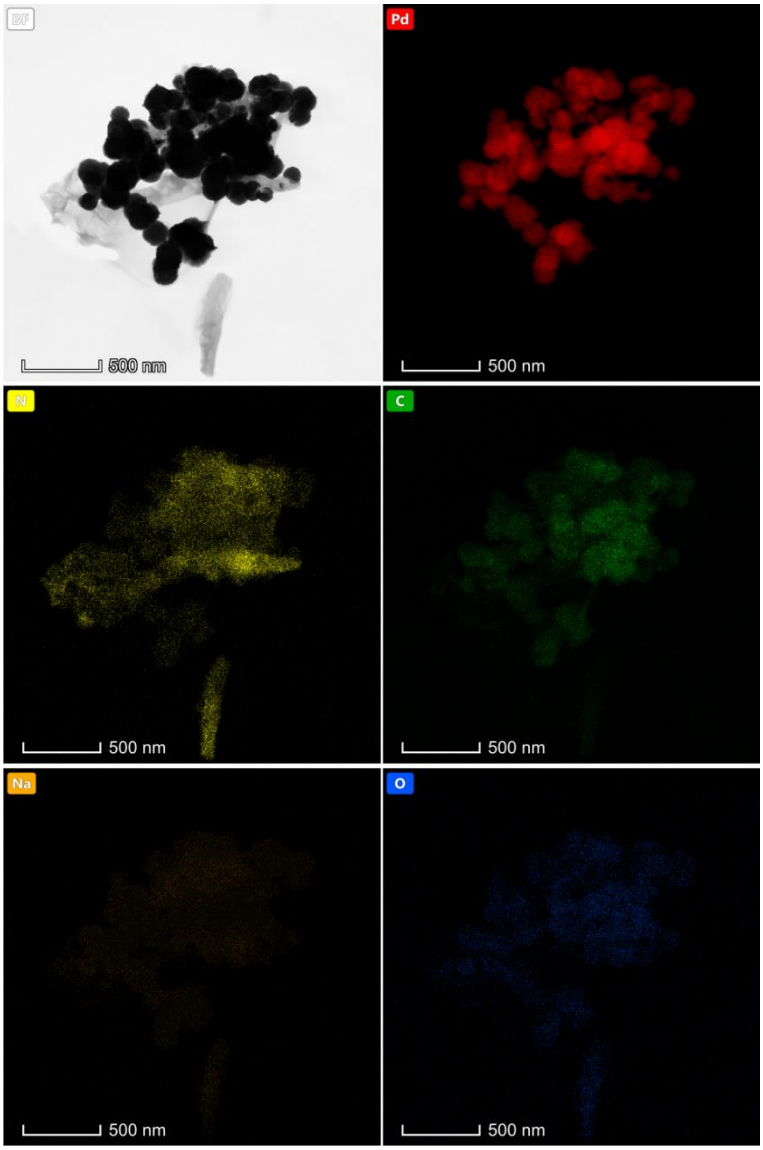

Figure 7. TEM image of the Pd/Na-g-C_3N_4 composite and distribution of palladium, carbon, nitrogen, sodium, and oxygen (in false colors).

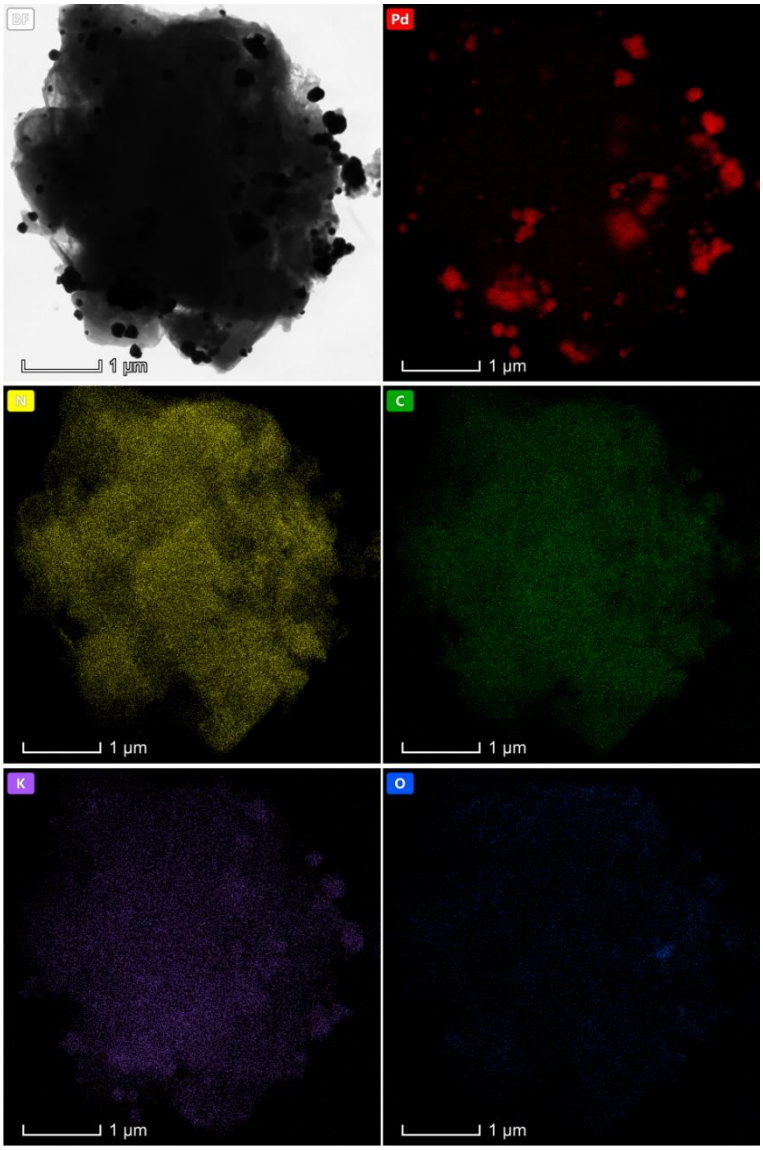

Figure 8. TEM image of Pd/K-g-C_3N_4 composite and distribution of palladium, carbon, nitrogen, potassium, and oxygen (in false colors).

X-ray photoelectron spectroscopy was used to evaluate the surface chemical composition of the studied composites. This analysis was applied for two kinds of samples: (i) before any photocatalytic process and (ii) after hydrogen generation processes conducted with the irradiation of 365 nm and 400 nm (discussed hereinafter). The latter analysis was performed in order to

observe whether any changes in chemical composition occurred during the process of photocatalytic hydrogen generation.

XPS investigations revealed the presence of C, N, O, and Pd in all samples. Dopant elements were identified in minor quantities. The detailed results are listed in Tables S1-4 in the Supplementary Materials.

Not surprisingly, the C 1s and N 1s spectra of all studied composites confirmed the presence of graphitic carbon nitride, as the most intense contributions arose from triazine rings [40,51–54]. The carbon content was always somewhat higher than the nominal value, resulting in a C:N ratio around 3.3:4 for the Pd/g-C_3N_4 composite and around 3.6:4 in the case of the composites on doped carbon nitride supports. However, no degradation of the g-C_3N_4 support was evident during the photocatalytic reaction, as both the characteristic binding energies and the line shapes of the carbon or nitrogen peaks remained unchanged.

The oxygen content of the samples was partly the result of the natural oxidation of the g-C_3N_4 material, as described in our previous work [38,40] and partly arose from oxidation of the Pd deposits.

Each sample contained sodium in ionic form (1071.4-1072 eV Na 1s). The origin of sodium in the materials is connected to the use of NaOH during the synthesis procedure. Importantly, in all cases, the content of sodium decreased after the photocatalytic process. It suggests that, in spite of washing the samples after the synthesis, some sodium-containing impurities still remained in them. In the case of Pd/Li-g-C_3N_4 and Pd/K-g-C_3N_4 composites, the ionic forms of Li and K have been found (54.5 eV Li 1s and 292.3-292.4 eV K $2p_{3/2}$, respectively). The content of potassium is not markedly changed after the photocatalytic process, whilst lithium before the process was not

detected because of the exact overlap of the expected position of the Li 1s peak with the rather broad Pd 4p peak and because of the close proximity of the Na 2s peak.

The apparent Pd content, as well as the chemical state data for Pd, are summarized in Table 3, while Pd 3d spectra of the fresh and used composites are shown in Figure 9.

Table 3. Summary of the results of the XPS analysis of the Pd/g-C_3N_4 composites

Sample	Fresh catalyst			Recovered catalyst[a]		
	Pd content (wt%)	Pd $3d_{5/2}$ binding energy (eV), chemical state		Pd content (wt%)	Pd $3d_{5/2}$ binding energy (eV), chemical state	
Pd/g-C_3N_4	22.9	338.1	Pd^{4+} ions in PdO_2 or oxyhydroxide	26.1	337.1	Pd^{2+} ions: PdO or oxyhydroxide
Pd/Li-g-C_3N_4	9.6	337.9	Pd^{4+} ions: PdO_2 or oxyhydroxide	7.6	335.4 338.2	metallic Pd Pd^{4+} ions
Pd/Na-g-C_3N_4	36.2	337.5 (broad)	Pd^{4+} and Pd^{2+} ions: PdO_2 and PdO or oxyhydroxides	23.5	337.7 (broad)	Pd^{4+} and Pd^{2+} ions: PdO_2 and PdO or oxyhydroxides
Pd/K-g-C_3N_4	8.7	335.2 337.5	metallic Pd Pd^{4+} and Pd^{2+} ions	6.6 4.5[b]	336.6 337.2[b] (broad)	Pd^{2+} ions: PdO or oxyhydroxides Pd^{4+} and Pd^{2+} ions

[a]: Data for recovered catalysts are obtained for UV-visible ($\lambda \geq 365$ nm) irradiation.

[b]: Measured after visible (400 nm) irradiation.

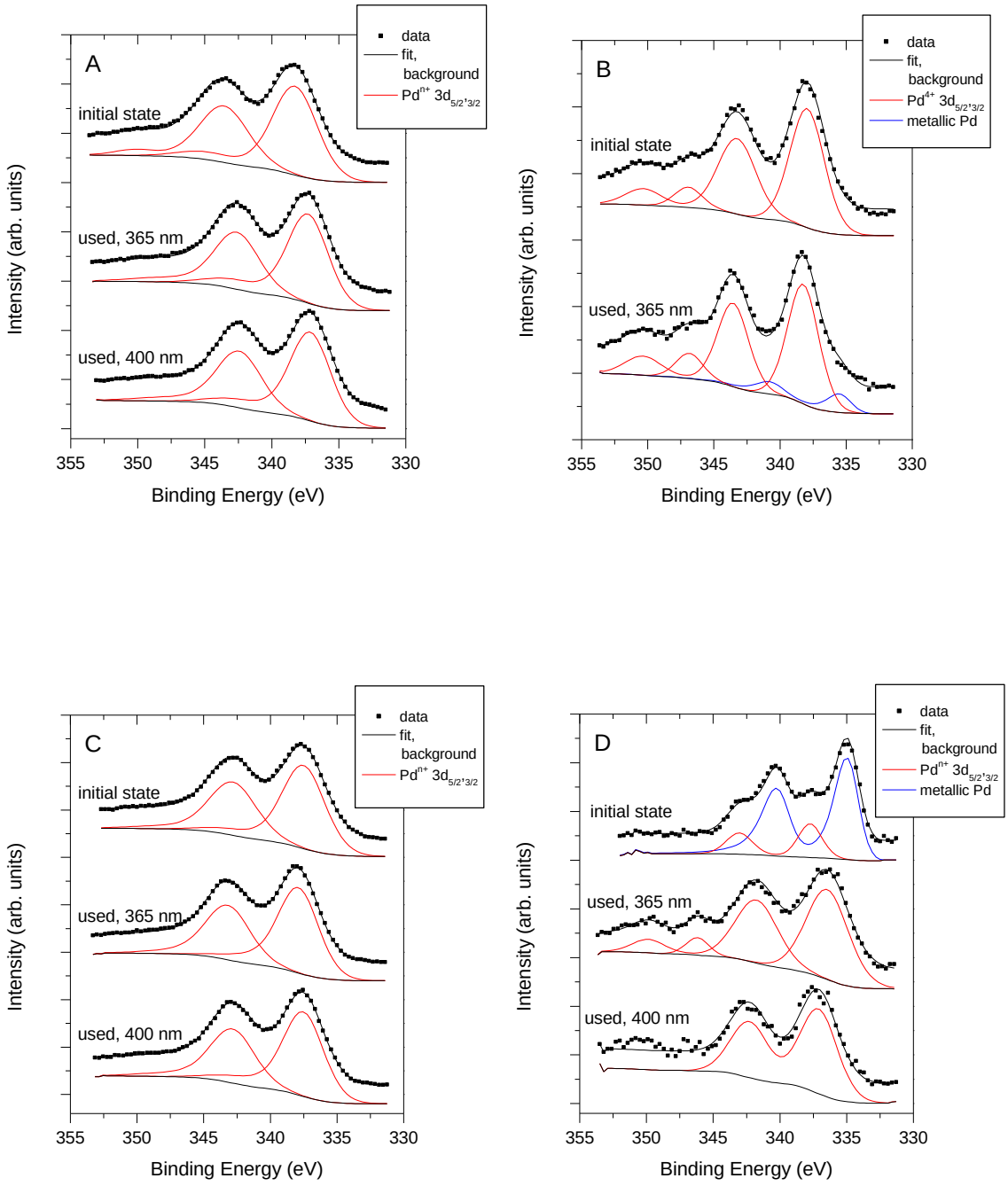

Figure 9. Pd 3d spectra of photocatalysts prepared on (A) undoped; (B) Li-doped; (C) Na-doped and (D) K-doped g-C_3N_4 supports.

For simplicity, in Table 3, data for the used catalysts were mainly measured after photocatalytic experiments with the UV-visible light source. The only exception is the Pd/K-g-C_3N_4 system,

where the UV-visible and the visible irradiation resulted in somewhat different Pd chemical states in the recovered catalysts (see also Tables S1-4 in the Supplementary Materials), Details of identification of the Pd chemical states can also be found in the Supplementary Materials.

Although the apparent Pd concentrations deduced from the XPS experiments are much higher than those measured by ICP-OES, the results are still reasonable if the structure of the samples is considered. In fact, if a metal catalyst is supported on the outer surface of a support, the apparent concentration of the metal measured by XPS will always be higher than the bulk (or nominal) concentration, and the difference increases with the dispersion of the metal. Thus, the high apparent Pd content of the Pd/g-C_3N_4 composite is in line with the relatively high dispersion of Pd, in agreement with the TEM results in Fig. 4 a) or Fig. 5. The somewhat worse Pd dispersion (see Fig. 4 b)) on the high surface area support leads to a significantly smaller apparent Pd content in the case of the Pd/Li-g-C_3N_4 composite. On the contrary, the relatively large coverage of big Pd agglomerates (Fig. 4 c), Fig. 7) on the low surface area Na-g-C_3N_4 support explains the unusually high apparent Pd content of the Pd/Na-g-C_3N_4 catalyst, while the decrease of the coverage (Fig. 8) is the reason of the much smaller apparent Pd content obtained for the Pd/K-g-C_3N_4 composite.

As it is shown in Figure 9 panel A, the Pd 3d spectrum of the fresh Pd/g-C_3N_4 composite consisted of a rather broad $3d_{5/2\text{-}3/2}$ spin-orbit doublet. Although the broad peaks may indicate the simultaneous presence of several chemical states, the $3d_{5/2}$ peak at 338.1 eV suggested the dominance of Pd^{4+} species arising from PdO_2 or $Pd(OH)_4$ probably surrounded by PdO [68,69] forming a hydrated Pd-oxide. A similarly broad and structureless Pd 3d envelope was observed in the used Pd/g-C_3N_4 composites, although the 1 eV shift of the $3d_{5/2}$ peak towards lower binding energies suggested a change in the distribution of the ionic Pd species in favor of the Pd^{2+} state [70–72]. It has to be mentioned that although Pd is a noble metal, its surface can be

reduced/oxidized relatively easily, especially in supported form. Thus, it is not surprising that the well dispersed Pd particles became highly oxidized upon ambient exposure in the fresh catalyst. The change in the oxidation state in the recovered catalysts indicates reduction under the reaction conditions, although assessing its extent is difficult because of the unavoidable re-oxidation after recovery.

The somewhat narrower $3d_{5/2\text{-}3/2}$ spin-orbit doublet of the fresh Pd/Li-g-C_3N_4 composite (Fig. 9 panel B) appeared at almost the same binding energy as in the case of the catalyst on the undoped support, indicating a similarly highly oxidized (Pd^{4+}) state, probably in hydroxide and/or oxyhydroxide environment. The spectrum of the recovered sample closely resembled that of the initial state, suggesting quite high stability of the Pd^{4+} ions. At the same time, a small (some 5-10% of the total Pd signal) contribution around 335.4 eV indicated the appearance of metallic Pd as a product of the photocatalytic reaction.

The $3d_{5/2}$ peak of the broad and very intense Pd 3d spectrum measured on the fresh Pd/Na-g-C_3N_4 composite (Figure 9, panel C) was observed around 337.5 eV binding energy, which is intermediate between those reported for Pd^{4+} (around 338 eV [68,69]) and Pd^{2+} (somewhat below 337 eV [70–72]). Thus, it is plausible to assume that a mixture of Pd^{2+} and Pd^{4+} ions is located at the surface of the sample. Although the TEM studies indicated the formation of large Pd agglomerates, the small primary particle size around 5 nm still can explain the sensitivity of the material towards oxidation upon air exposure. In the case of the recovered Pd/Na-g-C_3N_4 catalyst, neither the line shape nor the binding energy of the Pd 3d spectrum of the used samples differed significantly from those found in the initial state. Thus the Pd content remained the same mixture of Pd^{2+} and Pd^{4+} ionic states. Nevertheless, the presence of small amounts of metallic Pd or other

reduced forms cannot be ruled out, considering that their signals can easily be masked by the strong ionic contributions.

Finally, significantly different behavior was found for the Pd/K-g-C_3N_4 system (Pd 3d spectra depicted in Fig. 9, panel D). In the fresh state, a Pd $3d_{5/2}$ peak around 335 eV indicated that the Pd content was mainly metallic, completed by a mixture of Pd^{2+} and Pd^{4+} ions (smaller Pd $3d_{5/2}$ peak at 337.5 eV). Somewhat unexpectedly, in the recovered samples, predominantly ionic Pd species were observed, with a clear difference between the catalysts illuminated at different wavelengths. In the sample used in the UV-VIS photoreactor, the broad Pd $3d_{5/2}$ component was around 336.6 eV, suggesting a mainly Pd^{2+} ionic state, whilst the 337.2 eV binding energy for the sample illuminated at 400 nm indicated a mixture of Pd^{2+} and Pd^{4+} ionic states. At this stage, it is difficult to assess the effect of air exposure following the photocatalytic experiment. However, it is likely that the shorter wavelength illumination resulted in a more reduced but still ionic state in the K-doped samples.

The powder X-ray diffraction patterns of the studied materials (Figure 10) showed three reflections that perfectly fit metallic palladium [71,73]: (111) at 40.1°, (200) at 46.5°, and (220) at 66.7°. The broad peak located near 27° originates from the (002) g-C_3N_4 reflection [74]. XRD diffractograms of Pd/g-C_3N_4 composites containing the same reflections are shown elsewhere [26,27,30]. The investigation did not detect any other Pd-containing compounds, such as palladium oxide, palladium hydroxide, or palladium chloride. Nevertheless, the XRD results are in line with the XPS and TEM data. The weak metallic reflections in Pd/g-C_3N_4 are in agreement with the strongly oxidized nature of the well dispersed particles, while in Pd/Na-g-C_3N_4, the large agglomerates are evidenced by TEM must be mainly composed of small, heavily oxidized particles. The lack of oxide reflections probably indicates the disordered nature of the oxides. The

significant metallic Pd content of the Pd/K-g-C_3N_4 catalyst is confirmed by the XRD data, while in the Li-doped system, a few large metallic particles not detected by TEM may be responsible for the diffraction peaks. Surface sensitivity of XPS may also be a factor as it probes the depths up to 6-8 nm [75], whilst XRD analyzes the bulk samples.

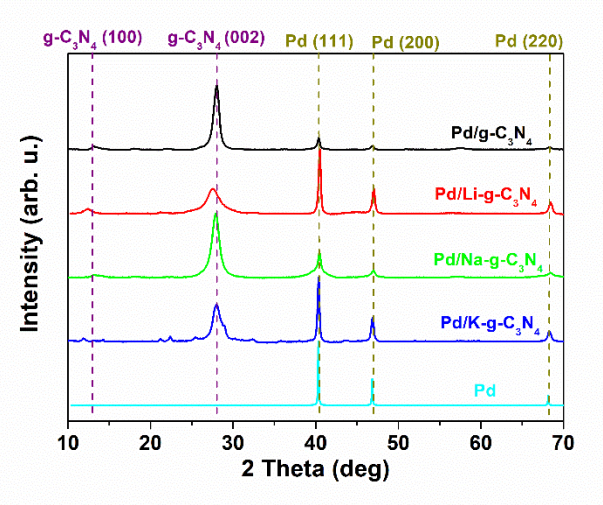

Figure 10. Powder X-ray diffractograms of the composites obtained and metallic Pd (as a reference). JCPDS cards: 05-0681 (Pd) and 87-1526 (g-C_3N_4).

The combination of structure and chemical state sensitive characterization methods, therefore, revealed a clear effect of the doping on the nature of the Pd deposits supported on the different g-C_3N_4 supports. The parent support and its Li-doped variant seemed to stabilize small but strongly oxidized Pd particles, although in the latter case, large metallic blocks not accessible for XPS must also be present. On the other hand, in the Na- and K-doped systems formation of large Pd-containing aggregates was preferred, probably not independently from the low specific surface area of the supports. Moreover, we found that the presence of a doping element in g-C_3N_4 had an effect on the redox behavior of Pd in their Pd-containing composites.

Variation in the surface chemistry of the doped supports is the probable reason for Pd loss during the photocatalytic measurements. Indeed, ICP-OES evidenced a significant decrease of the Pd content in the recovered catalysts for the Pd/Li-g-C_3N_4 and Pd/K-g-C_3N_4. Systems, most probably due to a combined effect of dissolution and mechanical abrasion. In these systems, which seem to facilitate the formation of large metallic Pd agglomerates, the particular surface properties [38] may result in weaker anchoring of Pd.

3.2. Photocatalytic behavior of g-C_3N_4 samples and Pd/g-C_3N_4 composites

3.2.1.Photodegradation of methyl orange.

The photodegradation of methyl orange was studied for the Pd-free and Pd-containing materials. Figure 11 presents the obtained kinetic curves for all studied materials (Figure S11 shows kinetics curves for each pair before and after the loading of Pd). Among Pd-free samples, the material doped with potassium exhibits the best photocatalytic performance because the concentration of dye decreased to a negligible level for the reaction time of ca. 4h, whilst for the other cases, after 6h, the solution still contains dye: 86% of the initial concentration in the case of Na-g-C_3N_4 and 28% for g-C_3N_4, respectively. No photodegradation was observed in lithium-doped graphitic carbon nitride. Plausibly, the band gap is too high, and the material comprising lithium is not able to catalyze the photodegradation reaction effectively. The composites with palladium exhibited different photocatalytic activities. The best performance was observed for the case of Pd/g-C_3N_4. In this case, the concentration of methyl orange decreased to 25% of the initial concentration. For the other cases, the observed concentration was as follows (in relation to the initial concentration): 37% (Pd/Na-g-C_3N_4), 65% (Pd/K-g-C_3N_4), and 91% (Pd/Li-g-C_3N_4). The construction of composite enhances the activity in two cases: lithium-doped and sodium-doped graphitic carbon

nitrides. For Li-g-C_3N_4 material, the enhancement is negligible. In the case of g-C_3N_4, the presence of Pd does not substantially modify the catalytic performance. Interestingly, the degradation process carried out over K-g-C_3N_4 was markedly hampered. The most important difference between Pd/K-g-C_3N_4 and other palladium-bearing composites is the much higher oxygen content on the surface (determined via XPS- Table S4), namely 16.5 at.%, whilst for the other samples, this value did not exceed 8.6 at.%. Thus, the surface of this sample is more oxidized, and plausibly, the surface of the palladium nanoparticles is also more oxidized. This feature significantly influences the catalytic performance of the material, making it less active.

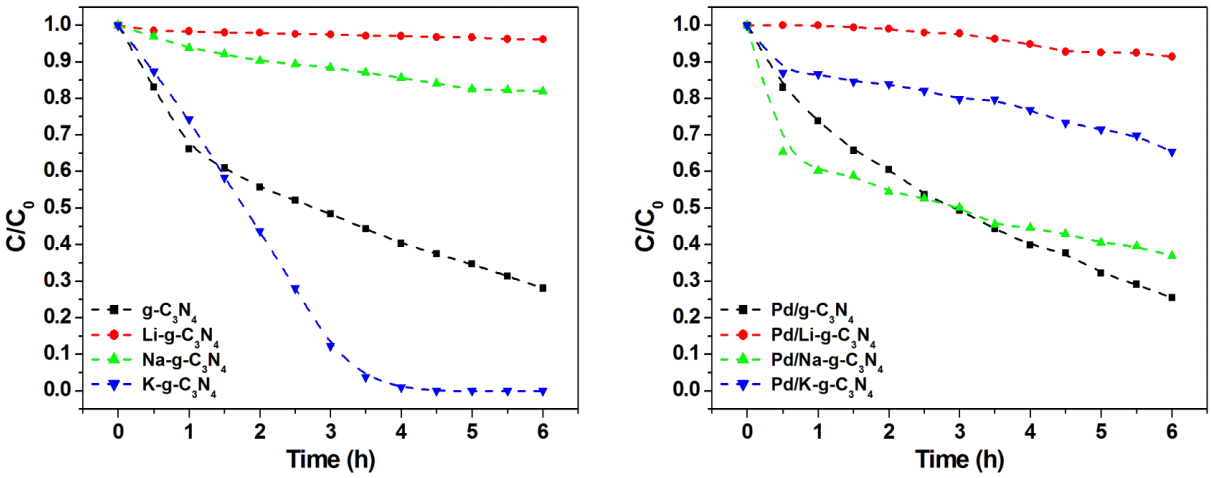

Figure 11. Kinetic curves of photodegradation of methyl orange over Pd-free samples and Pd-containing samples (right).

The kinetics data were fitted to the first-order kinetics: $C=C_0 \cdot e^{-kt}$, using its linear form: $-ln(C/C_0)=kt$. The obtained values of rate constants are shown in Table 4. The linear forms of kinetic curves fitted to the first-order model are shown in Figure S12. The kinetics of photodegradation of methyl blue perfectly fits the applied model in most cases because the correlation coefficient (R^2) is higher than 0.98. K-g-C_3N_4 exhibits weaker goodness of fit ($R^2=0.94$), only. The rate constants determined for the composites are higher than for the graphitic carbon nitrides, with an

exception for K-g-C_3N_4. This finding suggests that the construction of composites with palladium enhances the photocatalytic activity of the material. The obtained *k* values are in the range of 0.050-0.201 min^{-1} for the composites and 0.005-0.177 min^{-1} for the case of pure carbon nitrides. K-g-C_3N_4 is an exception because the determined rate constant is 1.225 min^{-1}.

Table 4. Determined first-order kinetics rate constants of the photodegradation of methyl blue.

Material	Pure material		Composite with Pd NPs	
	k (h^{-1})	R^2	k (h^{-1})	R^2
g-C_3N_4	0.177	0.993	0.207	0.998
Li-g-C_3N_4	0.005	0.995	0.018	0.980
Na-g-C_3N_4	0.030	0.989	0.101	0.995
K-g-C_3N_4	1.225	0.939	0.050	0.981

The photocatalytic removal of methyl orange was studied in many papers. Dong et al. [76] presented the photocatalytic performance of graphitic carbon nitride synthesized from melamine via polycondensation at 520°C. Importantly, they also obtained the oxidized g-C_3N_4 by solvothermal treatment of pristine material with the use of hydrogen peroxide. They showed that oxidation markedly enhances photocatalytic activity. The first order kinetics rate constants in their case were found to be 0.0105 and 0.1607 h^{-1} for the pristine and oxidized g-C_3N_4, respectively. However, they applied 0.1g of photocatalyst in 100 cm^3 of 10 $mg \cdot dm^{-3}$ methyl orange aqueous solution, whilst herein 1g of the photocatalyst and 300 cm^3 of dye solution were applied. Moreover, the power of irradiation in their case was 350 W. He et al. [77] synthesized the composite of g-C_3N_4 with MoO_3. The support was synthesized via polycondensation of melamine at 520°C. The first-order rate constant in the photodegradation of methyl orange in their case was found to be 0.0017 min^{-1} (0.102 h^{-1}), which is similar to the Pd/Na-g-C_3N_4 (0.101 h^{-1}). The power of irradiation was 350 W, the concentration of dye was 20 $mg \cdot dm^{-3}$, the mass of photocatalyst was 0.2 g, and the volume of solution was 100 cm^3. The comparison of the synthesized composites with the

previously studied materials shows that the composite Pd/g-C_3N_4 has better catalytic performance in the photodegradation of methyl orange. However, the best catalytic performance was found for the Pd-free K-doped graphitic carbon nitride.

3.2.2. Hydrogen generation in methanol photocatalytic reforming reaction

The hydrogen generation over the bare g-C_3N_4 could not be observed in our experimental setup. Therefore a direct comparison of the catalytic properties of the bare g-C_3N_4 materials was not feasible in this reaction. It is known that the photocatalytic methanol reforming reaction proceeds via the formation of stable intermediates such as formaldehyde and formic acid in the most frequently studied noble metal/TiO_2 systems [78–80]. It has to be noted that the present work was not addressed to mechanism studies; our aim was only the detection of the H_2 formation over the various Pd/g-C_3N_4 composites.

In general, the rate of H_2 production reactions can be increased at least one order of magnitude by deposition of metal cocatalysts on the surface of the semiconductor [81]. Consequently, the photocatalytic activity of metal-modified systems may be affected not only by the properties of the semiconductor but also by the properties of the cocatalyst. According to generally accepted opinions, deposited metal particles can increase the activity of the photocatalysts by decreasing the overvoltage of H_2 evolution [81,82]. In addition, decreasing the recombination of the photoexcited electron-hole pairs can also be taken into account because the metal NPs behave as electron traps through Schottky barrier formation [81,82]. Based on the literature analogies, the effective charge separation also has to been taken into account. Platinum as the co-catalyst resulted in the enhanced charge separation by transfer of photogenerated conduction band electrons on g-C_3N_4 into metal nanoparticles. [83,84]. The results of EIS measurements in a recent paper over a

series of g-C_3N_4, Na-g-C3N4, and Pt/Na-g-C_3N_4 samples presented that the radius of the arc in the spectra further decreased after Pt loading, confirming the most efficient electron-hole separation of the Pt/Na-g-C_3N_4 [24]. One of the effective metallic elements for photoreforming catalysts is palladium [85,86]. Although the Pd load was relatively high on all of our samples and the increase of the surface metal content beyond a certain limit is unfavorable according to the literature [87], the H_2 formation on these Pd-containing samples was well detectable.

Figure 12 shows the H_2 formation rate over Pd composites of undoped and doped g-C_3N_4-s under UV-Vis irradiation (Figure 12A) in Reactor UV and under visible light irradiation (Figure 12B) in Reactor VIS (see Figure S2 in Supplementary Materials). The H_2 formation rate-reaction time dependencies have two main parts, the initial period and a plateau in both systems. The plateau of the H_2 evolution rate represents the continuous formation of H_2. The gradual increase of the H_2 evolution rate in the initial period can be explained by at least two reasons: (i) the methanol solution should be first saturated by H_2 and reach equilibrium for the liquid phase/nitrogen flow before the measurement became relevant to real gas evolution; (ii) catalytically active sites are *in situ* formed which requires some time.

The rate of the photocatalytic H_2 production under UV-visible irradiation in reactor UV (Figure 12 A) showed the following order: Pd/Li-g-C_3N_4 < Pd/g-C_3N_4 < Pd/Na-g-C_3N_4 ~ Pd/K-g-C_3N_4.

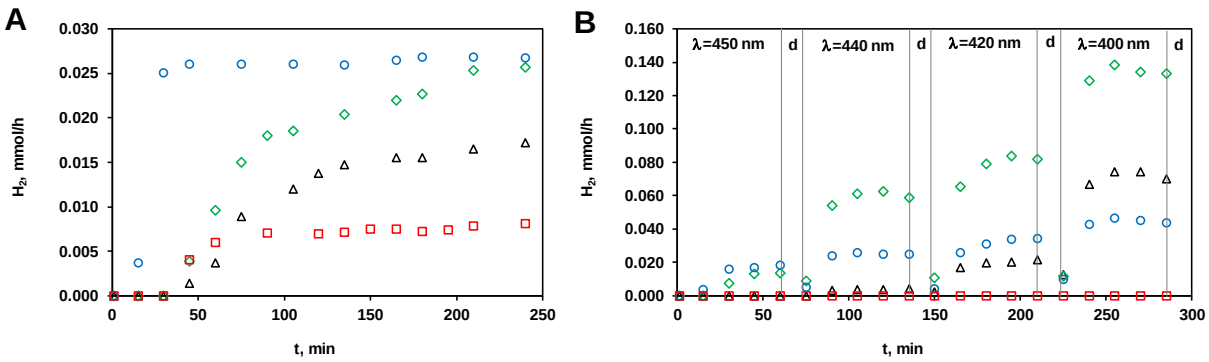

Figure 12. Time dependencies of photocatalytic H_2 formation. A: wavelength of irradiation ≥ 365 nm (Reactor UV); B: irradiation with visible light of different wavelengths (Reactor VIS). ○: Pd/K-g-C_3N_4, ◊: Pd/Na-g-C_3N, Δ: Pd/g-C_3N_4, □: Pd/Li-g-C_3N, d: dark period with stirring in Reactor VIS

Despite the different states of the Pd cocatalyst, this order was in good agreement with the order that can be estimated on the base of diffuse-reflectance UV-Vis spectroscopic measurements of the bare semiconductors. K- and Na-doping increased the evolution rate of H_2 by some 30% compared to the undoped sample, while Li-doping halved it. It is interesting to note that Pd/K-g-C_3N_4 had the shortest induction period of the kinetic curve, where metallic Pd on the surface of the fresh sample was indicated by XPS.

In the case of smaller energy of irradiation provided in Reactor VIS (Figure 12B), Pd/Li-g-C_3N was not active. Although this composite has the highest specific surface area [38], its light-absorbing properties were the poorest in the series of samples. In the case of Pd/Na-g-C_3N_4 and Pd/K-g-C_3N_4, the photocatalytic response has started at larger wavelengths (450, 440 nm) in accordance with their decreased band gap. The rate of H_2 formation on K-g-C_3N_4 was significantly lower than that measured on Na-g-C_3N_4. As can be seen in Figure 13, the repeated experiments gave the same trend. The reason for the observed phenomenon is not clear yet; some type of

passivation could be assumed for the K-doped sample when the irradiation energy was not sufficient at the beginning of the measurement (450 nm). Further investigations are needed to explain this observation.

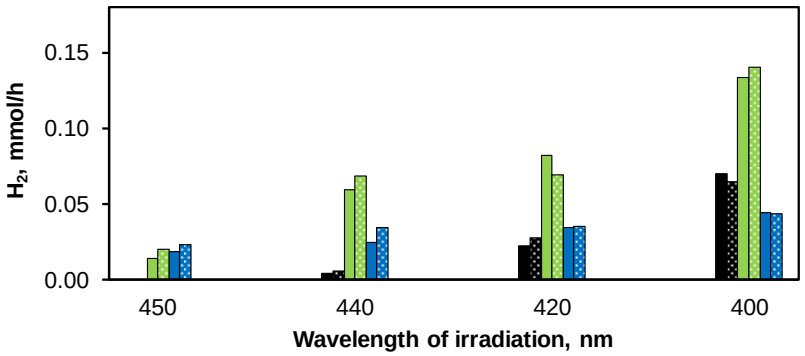

Figure 13. Comparison of results of parallel experiments hydrogen at irradiation with visible light (Reactor VIS). H_2 evolution rates measured after 60 min irradiation at given wavelength; black: Pd/undoped g-C_3N_4; green: Pd/Na doped g-C_3N_4; blue: Pd/K doped g-C_3N_4; column with texture: repeated experiment

In the next series of experiments with the Pd/K-g-C_3N_4 sample, the reaction time was increased from 60 min to 105 min at the first step, *i.e.*, at the lowest energy of irradiation (450 nm) in Reactor VIS, but no significant changes were resulted (cf. blue rings in Figure 12 and Figure 14). Then the irradiation, stirring and N_2 flow was switched off for 36 h. The restart gave very good reproducibility of H_2 production except for the first step, where the induction period was not observed. These results indicated the *in situ* formation of certain catalytic active sites and the reusability of the sample.

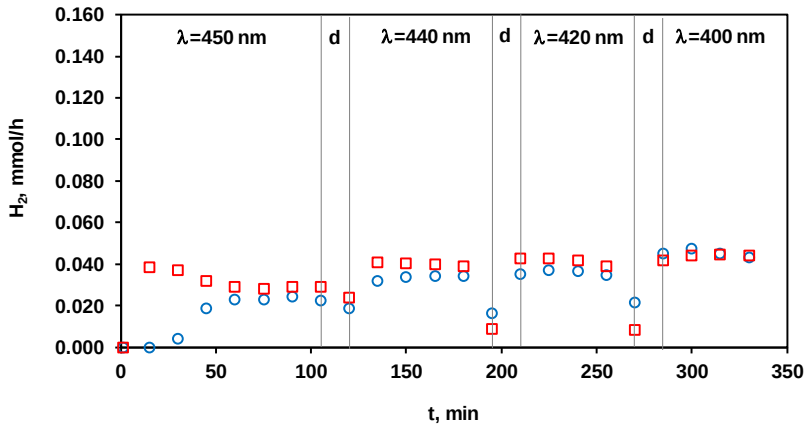

Figure 14. Photocatalytic H_2 formation on Pd/K-g-C_3N_4 composite in restarted irradiation in Reactor VIS. d: dark period with stirring, ○: the first series of irradiation, □: second series of radiation (36 hours after the first series, with an unstirred dark period)

Regarding the role of Pd, we did not find a direct correlation between the decrease of the total amount of Pd measured by ICP-OES in the recovered sample (Table 2) and the rate of photocatalytic H_2 production on these composites (data in Figure 12-13). It could be concluded that only a certain part of the introduced Pd was involved as a cocatalyst in our samples. According to the literature, the surface concentration of the cocatalyst has an optimum value [87] which is lower than it was in our case.

In general, small NPs in the metallic form are considered as active cocatalysts for H_2 production [88]. However, palladium particles with oxidized initial form were also described to behave as an appropriate cocatalyst for it [87,89]. It is known that calcination of supported Pd salts in air yields surface Pd-oxide [90], but Pd compounds on various semiconductors obtained after impregnation

followed by calcining give well-functioning cocatalysts. Their activity was explained by the easy reduction of the surface layer of the Pd-oxides [87].

We found that the presence of Pd^{2+} on the surface of the fresh composite or formation Pd^{2+} during the irradiation detected by XPS (Table S1-S4 in the Supplementary Materials) had a certain correlation with the photocatalytic hydrogen production. We assumed that Pd^{2+} could be easily reduced to dispersed (active) Pd on the surface. However, dispersed Pd^0 NPs could easily be oxidized during sample handling (recovering, XPS sample preparation). That is why we were not able to detect them after our sampling procedure. Based on these observations, we concluded that the really acting metallic Pd cocatalyst was formed mainly *in situ*. It has also been hypothesized that different irradiation energies result in different Pd surfaces when using one or the other reactor system.

Based on literature data [79] and on our results, a schematic model depicted in Figure 15 can be described for the methanol photocatalytic reforming reaction on our composites.

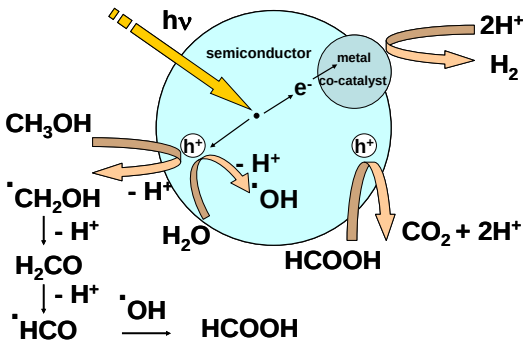

Figure 15. Schematic model of methanol photocatalytic reforming reaction

4. Conclusions

Herein, the composites of palladium NPs with graphitic carbon nitride have been synthesized and studied as prospective catalysts for hydrogen production. The novelty of this work stems from the doping of graphitic carbon nitride with alkali metals (Li, Na, K) before the Pd deposition. The presented synthesis route is simple and includes two steps: (i) synthesis of carbon nitride from cyanamide with or without metal doping and (ii) palladium loading via $PdCl_2$ reduction with L-ascorbic acid. Na- and K-doped graphitic carbon nitrides had decreased, while Li-doped graphitic carbon nitrides had enhanced band gap value compared to the undoped one. The content of the Pd in the composites was found to be about 4 wt%. Palladium has formed either dispersed (undoped g-C_3N_4, Li-g-C_3N_4) or agglomerated deposits (Na-g-C_3N_4, K-g-C_3N_4) with the primary particle size below 5nm. The aggregate formation of Pd could be related to the reduced specific surface area of the Na- and K-doped samples. The morphology and surface properties of the semiconductor affected the formation and stability of the cocatalyst; the same method of preparation led to different Pd composites in the case of the different dopants of the g-C_3N_4. The samples were studied in two tests: (i) photodegradation of methyl orange and (ii) hydrogen production via methanol reforming. The rate of the methyl orange degradation under visible light irradiation exhibited the order Pd/Li-g-C_3N_4 < Pd/K-g-C_3N_4 < Pd/Na-g-C_3N_4 < Pd/g-C_3N_4, and Li-g-C_3N_4 < Na-g-C_3N_4 < g-C_3N_4 < K-g-C_3N_4 for the bare semiconductors. The rate of the photocatalytic H_2 production under UV-visible irradiation showed the following order: Pd/Li-g-C_3N_4 < Pd/g-C_3N_4 < Pd/Na-g-C_3N_4 ~ Pd/K-g-C_3N_4 while bare g-C_3N_4-s did not give measurable H_2 formation. The carbon nitride matrix was found to be stable during the photocatalytic experiments, while the Pd part underwent certain changes during the photocatalytic reforming reaction of methanol. It could be concluded that only a certain part of the introduced Pd was involved as cocatalyst in the

methanol photocatalytic reforming reaction, and the really acting metallic Pd cocatalyst was formed mainly *in situ*. To sum up, the herein presented data demonstrate that the use of Na -doped g-C_3N_4 is a prospective method to enhance the photocatalytic performance in hydrogen production.

Acknowledgment

The research within project No.VEKOP-2.3.2-16-2017-00013 was supported by the European Union and the State of Hungary, co-financed by the European Regional Development Fund (András Tompos).

The authors thank Zoltán May for ICP-OES measurements.

REFERENCES

[1] A.Y. Liu, M.L. Cohen, Structural properties and electronic structure of low-compressibility materials: -Si3N4 and hypothetical -C3N4, Physical Review B. 41 (1990) 10727–10734. https://doi.org/10.1103/PhysRevB.41.10727.

[2] F. Goettmann, A. Fischer, M. Antonietti, A. Thomas, Chemical Synthesis of Mesoporous Carbon Nitrides Using Hard Templates and Their Use as a Metal-Free Catalyst for Friedel–Crafts Reaction of Benzene, Angewandte Chemie International Edition. 45 (2006) 4467–4471. https://doi.org/10.1002/anie.200600412.

[3] A. Thomas, A. Fischer, F. Goettmann, M. Antonietti, J.-O. Müller, R. Schlögl, J.M. Carlsson, Graphitic carbon nitride materials: variation of structure and morphology and their use as metal-free catalysts, Journal of Materials Chemistry. 18 (2008) 4893. https://doi.org/10.1039/b800274f.

[4] S.C. Yan, Z.S. Li, Z.G. Zou, Photodegradation performance of g-C3N4 fabricated by directly heating melamine, Langmuir. 25 (2009) 10397–10401. https://doi.org/10.1021/la900923z.

[5] S. Cao, J. Low, J. Yu, M. Jaroniec, Polymeric Photocatalysts Based on Graphitic Carbon Nitride, Advanced Materials. 27 (2015) 2150–2176. https://doi.org/10.1002/adma.201500033.

[6] N.S.N. Hasnan, M.A. Mohamed, Z.A. Mohd Hir, Surface Physicochemistry Modification and Structural Nanoarchitectures of g-C3N4 for Wastewater Remediation and Solar Fuel Generation, Advanced Materials Technologies. (2021). https://doi.org/10.1002/admt.202100993.

[7] G. Dong, Y. Zhang, Q. Pan, J. Qiu, A fantastic graphitic carbon nitride (g-C3N4) material: Electronic structure, photocatalytic and photoelectronic properties, Journal of Photochemistry and Photobiology C: Photochemistry Reviews. 20 (2014) 33–50. https://doi.org/10.1016/j.jphotochemrev.2014.04.002.

[8] M. Fronczak, Adsorption performance of graphitic carbon nitride-based materials: Current state of the art, Journal of Environmental Chemical Engineering. 8 (2020) 104411. https://doi.org/10.1016/j.jece.2020.104411.

[9] X. Wang, K. Maeda, A. Thomas, K. Takanabe, G. Xin, J.M. Carlsson, K. Domen, M. Antonietti, A metal-free polymeric photocatalyst for hydrogen production from water under visible light, Nature Materials. 8 (2009) 76–80. https://doi.org/10.1038/nmat2317.

[10] X. Zou, R. Silva, A. Goswami, T. Asefa, Cu-doped carbon nitride: Bio-inspired synthesis of H2-evolving electrocatalysts using graphitic carbon nitride (g-C3N4) as a host material, Applied Surface Science. 357 (2015) 221–228. https://doi.org/10.1016/j.apsusc.2015.08.197.

[11] X. Wang, K. Maeda, X. Chen, K. Takanabe, K. Domen, Y. Hou, X. Fu, M. Antonietti, Polymer Semiconductors for Artificial Photosynthesis: Hydrogen Evolution by Mesoporous Graphitic Carbon Nitride with Visible Light, Journal of the American Chemical Society. 131 (2009) 1680–1681. https://doi.org/10.1021/ja809307s.

[12] X. She, L. Liu, H. Ji, Z. Mo, Y. Li, L. Huang, D. Du, H. Xu, H. Li, Template-free synthesis of 2D porous ultrathin nonmetal-doped g-C3N4 nanosheets with highly efficient photocatalytic H2 evolution from water under visible light, Applied Catalysis B: Environmental. 187 (2016) 144–153. https://doi.org/10.1016/j.apcatb.2015.12.046.

[13] S. Le, T. Jiang, Y. Li, Q. Zhao, Y. Li, W. Fang, M. Gong, Highly efficient visible-light-driven mesoporous graphitic carbon nitride/ZnO nanocomposite photocatalysts, Applied Catalysis B: Environmental. 200 (2017) 601–610. https://doi.org/10.1016/j.apcatb.2016.07.027.

[14] Y. Zheng, Z. Zhang, C. Li, A comparison of graphitic carbon nitrides synthesized from different precursors through pyrolysis, Journal of Photochemistry and Photobiology A: Chemistry. 332 (2017) 32–44. https://doi.org/10.1016/j.jphotochem.2016.08.005.

[15] F. Chang, Y. Xie, C. Li, J. Chen, J. Luo, X. Hu, J. Shen, A facile modification of g-C 3 N 4 with enhanced photocatalytic activity for degradation of methylene blue, Applied Surface Science. 280 (2013) 967–974. https://doi.org/10.1016/j.apsusc.2013.05.127.

[16] Y. Wang, X. Wang, M. Antonietti, Polymeric graphitic carbon nitride as a heterogeneous organocatalyst: From photochemistry to multipurpose catalysis to sustainable chemistry, Angewandte Chemie - International Edition. 51 (2012) 68–89. https://doi.org/10.1002/anie.201101182.

[17] R. Thankam Thomas, N. Sandhyarani, Template free synthesis of graphitic carbon nitride/titania mesoflowers, RSC Advances. 5 (2015) 72683–72690. https://doi.org/10.1039/c5ra14547c.

[18] S. Zhou, Y. Liu, J. Li, Y. Wang, G. Jiang, Z. Zhao, D. Wang, A. Duan, J. Liu, Y. Wei, Facile in situ synthesis of graphitic carbon nitride (g-C3N4)-N-TiO2 heterojunction as an efficient photocatalyst for the selective photoreduction of CO2 to CO, Applied Catalysis B: Environmental. 158–159 (2014) 20–29. https://doi.org/10.1016/j.apcatb.2014.03.037.

[19] M. Xu, L. Han, S. Dong, Facile Fabrication of Highly Efficient g-C 3 N 4 /Ag 2 O Heterostructured Photocatalysts with Enhanced Visible-Light Photocatalytic Activity, ACS Applied Materials & Interfaces. 5 (2013) 12533–12540. https://doi.org/10.1021/am4038307.

[20] C. Xu, P. Qiu, H. Chen, Y. Zhou, F. Jiang, X. Xie, Pd/mesoporous carbon nitride: A bifunctional material with high adsorption capacity and catalytic hydrodebromination activity for removal of tetrabromobisphenol A, Colloids and Surfaces A: Physicochemical and Engineering Aspects. 506 (2016) 654–663. https://doi.org/10.1016/j.colsurfa.2016.07.050.

[21] L. Liu, X. Wu, L. Wang, X. Xu, L. Gan, Z. Si, J. Li, Q. Zhang, Y. Liu, Y. Zhao, R. Ran, X. Wu, D. Weng, F. Kang, Atomic palladium on graphitic carbon nitride as a hydrogen evolution catalyst under visible light irradiation, Communications Chemistry. 2 (2019) 2–9. https://doi.org/10.1038/s42004-019-0117-4.

[22] H.W. Zuo, C.H. Lu, Y.R. Ren, Y. Li, Y.F. Zhang, W.K. Chen, Pt4 clusters supported on monolayer graphitic carbon nitride sheets for oxygen adsorption: A first-principles study, Wuli Huaxue Xuebao/ Acta Physico - Chimica Sinica. 32 (2016) 1183–1190. https://doi.org/10.3866/PKU.WHXB201603032.

[23] S. Cao, J. Jiang, B. Zhu, J. Yu, Shape-dependent photocatalytic hydrogen evolution activity over a Pt nanoparticle coupled g-C3N4 photocatalyst, Physical Chemistry Chemical Physics. 18 (2016) 19457–19463. https://doi.org/10.1039/c6cp02832b.

[24] F. Liang, X. Sun, S. Hu, H. Ma, F. Wang, G. Wu, Photocatalytic water splitting to simultaneously produce H2 and H2O2 by two-electron reduction process over Pt loaded Na+ introduced g-C3N4 catalyst, Diamond and Related Materials. 108 (2020). https://doi.org/10.1016/j.diamond.2020.107971.

[25] L.L. Zhang, L.L. Zhang, S. Cheng, X. Zhou, N. Shang, S. Gao, C. Wang, Pd supported on graphene modified g-C 3 N 4 hybrid: a highly efficient catalyst for hydrogenation of nitroarenes, Applied Organometallic Chemistry. 34 (2020). https://doi.org/10.1002/aoc.5684.

[26] Y. Zhao, R. Tang, R. Huang, Palladium Supported on Graphitic Carbon Nitride: An Efficient and Recyclable Heterogeneous Catalyst for Reduction of Nitroarenes and Suzuki Coupling Reaction, Catalysis Letters. 145 (2015) 1961–1971. https://doi.org/10.1007/s10562-015-1600-x.

[27] J. Sun, Y. Fu, G. He, X. Sun, X. Wang, Green Suzuki-Miyaura coupling reaction catalyzed by palladium nanoparticles supported on graphitic carbon nitride, Applied Catalysis B: Environmental. 165 (2015) 661–667. https://doi.org/10.1016/j.apcatb.2014.10.072.

[28] W. Zhang, H. Huang, F. Li, K. Deng, X. Wang, Palladium nanoparticles supported on graphitic carbon nitride-modified reduced graphene oxide as highly efficient catalysts for formic acid and methanol electrooxidation, Journal of Materials Chemistry A. 2 (2014) 19084–19094. https://doi.org/10.1039/c4ta03326d.

[29] C. Chang, Y. Fu, M. Hu, C. Wang, G. Shan, L. Zhu, Photodegradation of bisphenol A by highly stable palladium-doped mesoporous graphite carbon nitride (Pd/mpg-C3N4) under simulated solar light irradiation, Applied Catalysis B: Environmental. 142–143 (2013) 553–560. https://doi.org/10.1016/j.apcatb.2013.05.044.

[30] T. Bhowmik, M.K. Kundu, S. Barman, Palladium Nanoparticle-Graphitic Carbon Nitride Porous Synergistic Catalyst for Hydrogen Evolution/Oxidation Reactions over a Broad Range of pH and Correlation of Its Catalytic Activity with Measured Hydrogen Binding Energy, ACS Catalysis. 6 (2016) 1929–1941. https://doi.org/10.1021/acscatal.5b02485.

[31] Y.Z. Abdullahi, T.L. Yoon, R.E.A. Mohammad, Selective hydrogen adsorption on a buckled carbon nitride sheet: First-principles calculation, Materials Research Express. 5 (2018). https://doi.org/10.1088/2053-1591/aae1c1.

[32] A.A.S. Nair, R. Sundara, N. Anitha, Hydrogen storage performance of palladium nanoparticles decorated graphitic carbon nitride, International Journal of Hydrogen Energy. 40 (2015) 3259–3267. https://doi.org/10.1016/j.ijhydene.2014.12.065.

[33] J. Zhang, S. Hu, Y. Wang, A convenient method to prepare a novel alkali metal sodium doped carbon nitride photocatalyst with a tunable band structure, RSC Advances. 4 (2014) 62912–62919. https://doi.org/10.1039/c4ra11377b.

[34] Y. Zhang, S. Zong, C. Cheng, J. Shi, X. Guan, Y. Lu, L. Guo, One-pot annealing preparation of Na-doped graphitic carbon nitride from melamine and organometallic sodium salt for enhanced photocatalytic H2 evolution, International Journal of Hydrogen Energy. 43 (2018) 13953–13961. https://doi.org/10.1016/j.ijhydene.2018.04.042.

[35] W. Fang, J. Liu, L. Yu, Z. Jiang, W. Shangguan, Novel (Na, O) co-doped g-C3N4 with simultaneously enhanced absorption and narrowed bandgap for highly efficient hydrogen evolution, Applied Catalysis B: Environmental. 209 (2017) 631–636. https://doi.org/10.1016/j.apcatb.2017.03.041.

[36] S. Hu, F. Li, Z. Fan, F. Wang, Y. Zhao, Z. Lv, Band gap-tunable potassium doped graphitic carbon nitride with enhanced mineralization ability, Dalton Transactions. 44 (2014) 1084–1092. https://doi.org/10.1039/c4dt02658f.

[37] H. Sudrajat, A one-pot, solid-state route for realizing highly visible light active Na-doped gC3N4 photocatalysts, Journal of Solid State Chemistry. 257 (2018) 26–33. https://doi.org/10.1016/j.jssc.2017.09.024.

[38] M. Fronczak, K. Demby, P. Strachowski, M. Strawski, M. Bystrzejewski, Graphitic Carbon Nitride Doped with the s-Block Metals: Adsorbent for the Removal of Methyl Blue and Copper(II) Ions, Langmuir. 34 (2018) 7272–7283. https://doi.org/10.1021/acs.langmuir.8b01041.

[39] T. Xiong, W. Cen, Y. Zhang, F. Dong, Bridging the g-C3N4 Interlayers for Enhanced Photocatalysis, ACS Catalysis. 6 (2016) 2462–2472. https://doi.org/10.1021/acscatal.5b02922.

[40] M. Fronczak, M. Krajewska, K. Demby, M. Bystrzejewski, Extraordinary Adsorption of Methyl Blue onto Sodium-Doped Graphitic Carbon Nitride, Journal of Physical Chemistry C. 121 (2017) 15756–15766. https://doi.org/10.1021/acs.jpcc.7b03674.

[41] X. Song, H. Tao, L. Chen, Y. Sun, Synthesis of Fe/g-C3N4 composites with improved visible light photocatalytic activity, Materials Letters. 116 (2014) 265–267. https://doi.org/10.1016/j.matlet.2013.11.043.

[42] X. Rong, F. Qiu, J. Rong, X. Zhu, J. Yan, D. Yang, Enhanced visible light photocatalytic activity of W-doped porous g-C3N4 and effect of H2O2, Materials Letters. 164 (2016) 127–131. https://doi.org/10.1016/j.matlet.2015.10.131.

[43] J. Mu, J. Li, X. Zhao, E.C. Yang, X.J. Zhao, Cobalt-doped graphitic carbon nitride with enhanced peroxidase-like activity for wastewater treatment, RSC Advances. 6 (2016) 35568–35576. https://doi.org/10.1039/c6ra02911f.

[44] T. Xiong, W. Cen, Y. Zhang, F. Dong, Bridging the g-C3N4 Interlayers for Enhanced Photocatalysis, ACS Catalysis. 6 (2016) 2462–2472. https://doi.org/10.1021/acscatal.5b02922.

[45] B. Yue, Q. Li, H. Iwai, T. Kako, J. Ye, Hydrogen production using zinc-doped carbon nitride catalyst irradiated with visible light, Science and Technology of Advanced Materials. 12 (2011) 034401. https://doi.org/10.1088/1468-6996/12/3/034401.

[46] M.A. Mohamed, M.F. M. Zain, L. Jeffery Minggu, M.B. Kassim, N.A. Saidina Amin, W.N. W. Salleh, M.N.I. Salehmin, M.F. Md Nasir, Z.A. Mohd Hir, Constructing bio-templated 3D porous microtubular C-doped g-C3N4 with tunable band structure and enhanced charge carrier separation, Applied Catalysis B: Environmental. 236 (2018) 265–279. https://doi.org/10.1016/j.apcatb.2018.05.037.

[47] L. Jiang, X. Yuan, Y. Pan, J. Liang, G. Zeng, Z. Wu, H. Wang, Doping of graphitic carbon nitride for photocatalysis: A reveiw, Applied Catalysis B: Environmental. 217 (2017) 388–406. https://doi.org/10.1016/j.apcatb.2017.06.003.

[48] P.W. Chen, K. Li, Y.X. Yu, W. De Zhang, Cobalt-doped graphitic carbon nitride photocatalysts with high activity for hydrogen evolution, Applied Surface Science. 392 (2017) 608–615. https://doi.org/10.1016/j.apsusc.2016.09.086.

[49] Y. Wang, Y. Wang, Y. Chen, C. Yin, Y. Zuo, L.F. Cui, Synthesis of Ti-doped graphitic carbon nitride with improved photocatalytic activity under visible light, Materials Letters. 139 (2015) 70–72. https://doi.org/10.1016/j.matlet.2014.10.008.

[50] R. Mozingo, Palladium Catalysts, Organic Syntheses. 26 (1946) 77. https://doi.org/10.15227/orgsyn.026.0077.

[51] W.J. Gammon, O. Kraft, A.C. Reilly, B.C. Holloway, Experimental comparison of N(1s) X-ray photoelectron spectroscopy binding energies of hard and elastic amorphous carbon nitride films with reference organic compounds, Carbon. 41 (2003) 1917–1923. https://doi.org/10.1016/S0008-6223(03)00170-2.

[52] F. Dong, Z. Zhao, T. Xiong, Z. Ni, W. Zhang, Y. Sun, W.-K. Ho, In Situ Construction of g-C 3 N 4 /g-C 3 N 4 Metal-Free Heterojunction for Enhanced Visible-Light Photocatalysis, ACS Applied Materials & Interfaces. 5 (2013) 11392–11401. https://doi.org/10.1021/am403653a.

[53] S.C. Yan, Z.S. Li, Z.G. Zou, Photodegradation of Rhodamine B and Methyl Orange over Boron-Doped g-C 3 N 4 under Visible Light Irradiation, Langmuir. 26 (2010) 3894–3901. https://doi.org/10.1021/la904023j.

[54] D. Gao, Y. Liu, P. Liu, M. Si, D. Xue, Atomically Thin B doped g-C3N4 Nanosheets: High-Temperature Ferromagnetism and calculated Half-Metallicity, Scientific Reports. 6 (2016) 35768. https://doi.org/10.1038/srep35768.

[55] M. Mohai, XPS MultiQuant: multimodel XPS quantification software, Surface and Interface Analysis. 36 (2004) 828–832. https://doi.org/10.1002/sia.1775.

[56] H. Kisch, On the Problem of Comparing Rates or Apparent Quantum Yields in Heterogeneous Photocatalysis, Angewandte Chemie International Edition. 49 (2010) 9588–9589. https://doi.org/10.1002/anie.201002653.

[57] N. Jasni, A. Iqbal, M. Norazmi Ahmad, H. Pauzi, M.H. Hussain, Synthesis and characterisation of Li-modified g-C3N4, Materials Today: Proceedings. (2021). https://doi.org/10.1016/j.matpr.2021.10.086.

[58] A.B. Murphy, Bandgap determination from diffuse reflectance measurements of semiconductor films, and application to photoelectrochemical water-splitting, Solar Energy Materials and Solar Cells. 91 (2007) 1326–1337. https://doi.org/10.1016/j.solmat.2007.05.005.

[59] J. Tauc, Optical properties and electronic structure of amorphous Ge and Si, Materials Research Bulletin. 3 (1968) 37–46. https://doi.org/10.1016/0025-5408(68)90023-8.

[60] P. Kubelka, F. Munk, Ein Beitrag Zur Optik Der Farbanstriche, Zeitschrift Für Technische Physik. 12 (1931) 593–601.

[61] S. Valencia, J.M. Marín, G. Restrepo, Study of the bandgap of synthesized titanium dioxide nanoparticules using the sol-gel method and a hydrothermal treatment, Open Materials Science Journal. 4 (2010) 9–14. https://doi.org/10.2174/1874088X01004020009.

[62] Y. Di, X. Wang, A. Thomas, M. Antonietti, Making Metal-Carbon Nitride Heterojunctions for Improved Photocatalytic Hydrogen Evolution with Visible Light, ChemCatChem. 2 (2010) 834–838. https://doi.org/10.1002/cctc.201000057.

[63] V. Chakrapani, Semiconductor Junctions, Solid-Solid Junctions, in: Encyclopedia of Applied Electrochemistry, Springer New York, New York, NY, 2014: pp. 1882–1893. https://doi.org/10.1007/978-1-4419-6996-5_44.

[64] B. Zhu, P. Xia, Y. Li, W. Ho, J. Yu, Fabrication and photocatalytic activity enhanced mechanism of direct Z-scheme g-C 3 N 4 /Ag 2 WO 4 photocatalyst, Applied Surface Science. 391 (2017) 175–183. https://doi.org/10.1016/j.apsusc.2016.07.104.

[65] Q. Liu, J. Zhang, Graphene Supported Co-g-C 3 N 4 as a Novel Metal–Macrocyclic Electrocatalyst for the Oxygen Reduction Reaction in Fuel Cells, Langmuir. 29 (2013) 3821–3828. https://doi.org/10.1021/la400003h.

[66] I. Benisti, F. Shaik, Z. Xing, A. Ben-refael, L. Amirav, Y. Paz, The effect of Pt cocatalyst on the performance and transient IR spectrum of photocatalytic g-C3N4 nanospheres, Applied Surface Science. 542 (2021) 148432. https://doi.org/10.1016/j.apsusc.2020.148432.

[67] R.J. Farrauto, M.C. Hobson, T. Kennelly, E.M. Waterman, Catalytic chemistry of supported palladium for combustion of methane, Applied Catalysis A: General. 81 (1992) 227–237. https://doi.org/10.1016/0926-860X(92)80095-T.

[68] L.S. Kibis, A.I. Titkov, A.I. Stadnichenko, S.V. Koscheev, A.I. Boronin, X-ray photoelectron spectroscopy study of Pd oxidation by RF discharge in oxygen, Applied Surface Science. 255 (2009) 9248–9254. https://doi.org/10.1016/j.apsusc.2009.07.011.

[69] R. Rahul, R.K. Singh, B. Bera, R. Devivaraprasad, M. Neergat, The role of surface oxygenated-species and adsorbed hydrogen in the oxygen reduction reaction (ORR) mechanism and product selectivity on Pd-based catalysts in acid media, Physical Chemistry Chemical Physics. 17 (2015) 15146–15155. https://doi.org/10.1039/C5CP00692A.

[70] M. Brun, A. Berthet, J.C. Bertolini, XPS, AES and Auger parameter of Pd and PdO, Journal of Electron Spectroscopy and Related Phenomena. 104 (1999) 55–60. https://doi.org/10.1016/S0368-2048(98)00312-0.

[71] M. Fronczak, A. Kasprzak, M. Bystrzejewski, Carbon-encapsulated iron nanoparticles with deposited Pd: A high-performance catalyst for hydrogenation of nitro compounds, Journal of Environmental Chemical Engineering. 9 (2021) 104673. https://doi.org/10.1016/j.jece.2020.104673.

[72] Z. Wu, Z. Sheng, H. Wang, Y. Liu, Relationship between Pd oxidation states on TiO2 and the photocatalytic oxidation behaviors of nitric oxide, Chemosphere. 77 (2009) 264–268. https://doi.org/10.1016/j.chemosphere.2009.07.060.

[73] L.W. McKeehan, The Crystal Structures of the System Palladium-Hydrogen, Physical Review. 21 (1923) 334–342. https://doi.org/10.1103/PhysRev.21.334.

[74] T. Tyborski, C. Merschjann, S. Orthmann, F. Yang, M.C. Lux-Steiner, T. Schedel-Niedrig, Crystal structure of polymeric carbon nitride and the determination of its process-temperature-induced modifications, Journal of Physics Condensed Matter. 25 (2013) 395402. https://doi.org/10.1088/0953-8984/25/39/395402.

[75] J. Watts, J. Wolstenholme, An introduction to surface analysis by XPS and AES, J. Wiley, New York, 2003.

[76] G. Dong, Z. Ai, L. Zhang, Efficient anoxic pollutant removal with oxygen functionalized graphitic carbon nitride under visible light, RSC Advances. 4 (2014) 5553–5560. https://doi.org/10.1039/c3ra46068a.

[77] Y. He, L. Zhang, X. Wang, Y. Wu, H. Lin, L. Zhao, W. Weng, H. Wan, M. Fan, Enhanced photodegradation activity of methyl orange over Z-scheme type MoO3-g-C3N4 composite under visible light irradiation, RSC Advances. 4 (2014) 13610–13619. https://doi.org/10.1039/c4ra00693c.

[78] T.A. Kandiel, R. Dillert, L. Robben, D.W. Bahnemann, Photonic efficiency and mechanism of photocatalytic molecular hydrogen production over platinized titanium dioxide from aqueous methanol solutions, Catalysis Today. 161 (2011) 196–201. https://doi.org/10.1016/j.cattod.2010.08.012.

[79] W.-C. Lin, W.-D. Yang, I.-L. Huang, T.-S. Wu, Z.-J. Chung, Hydrogen Production from Methanol/Water Photocatalytic Decomposition Using Pt/TiO 2− x N x Catalyst, Energy & Fuels. 23 (2009) 2192–2196. https://doi.org/10.1021/ef801091p.

[80] G.L. Chiarello, D. Ferri, E. Selli, Effect of the CH3OH/H2O ratio on the mechanism of the gas-phase photocatalytic reforming of methanol on noble metal-modified TiO2, Journal of Catalysis. 280 (2011) 168–177. https://doi.org/10.1016/j.jcat.2011.03.013.

[81] J. Yang, D. Wang, H. Han, C. Li, Roles of Cocatalysts in Photocatalysis and Photoelectrocatalysis, Accounts of Chemical Research. 46 (2013) 1900–1909. https://doi.org/10.1021/ar300227e.

[82] A.L. Linsebigler, G. Lu, J.T. Yates, Photocatalysis on TiO2 Surfaces: Principles, Mechanisms, and Selected Results, Chemical Reviews. 95 (1995) 735–758. https://doi.org/10.1021/cr00035a013.

[83] Y. Shiraishi, Y. Kofuji, S. Kanazawa, H. Sakamoto, S. Ichikawa, S. Tanaka, T. Hirai, Platinum nanoparticles strongly associated with graphitic carbon nitride as efficient cocatalysts for photocatalytic hydrogen evolution under visible light, Chem. Commun. 50 (2014) 15255–15258. https://doi.org/10.1039/C4CC06960A.

[84] M. Zhang, X. Wang, Two dimensional conjugated polymers with enhanced optical absorption and charge separation for photocatalytic hydrogen evolution, Energy & Environmental Science. 7 (2014) 1902. https://doi.org/10.1039/c3ee44189j.

[85] A. V. Puga, Photocatalytic production of hydrogen from biomass-derived feedstocks, Coordination Chemistry Reviews. 315 (2016) 1–66. https://doi.org/10.1016/j.ccr.2015.12.009.

[86] Y. Yao, X. Gao, Z. Li, X. Meng, Photocatalytic Reforming for Hydrogen Evolution: A Review, Catalysts. 10 (2020) 335. https://doi.org/10.3390/catal10030335.

[87] L.S. Al-Mazroai, M. Bowker, P. Davies, A. Dickinson, J. Greaves, D. James, L. Millard, The photocatalytic reforming of methanol, Catalysis Today. 122 (2007) 46–50. https://doi.org/10.1016/j.cattod.2007.01.022.

[88] L. Xu, S. Wang, T. Zhang, F. Chen, Photo-induced re-modulation of Pt particles loaded on V-TiO 2 for enhanced CO photocatalytic oxidation, Catalysis Science & Technology. 7 (2017) 3698–3701. https://doi.org/10.1039/C7CY01220A.

[89] K. Maeda, K. Teramura, N. Saito, Y. Inoue, K. Domen, Improvement of photocatalytic activity of (Ga1−xZnx)(N1−xOx) solid solution for overall water splitting by co-loading Cr and another transition metal, Journal of Catalysis. 243 (2006) 303–308. https://doi.org/10.1016/j.jcat.2006.07.023.

[90] J. Panpranot, O. Tangjitwattakorn, P. Praserthdam, J.G. Goodwin, Effects of Pd precursors on the catalytic activity and deactivation of silica-supported Pd catalysts in liquid phase hydrogenation, Applied Catalysis A: General. 292 (2005) 322–327. https://doi.org/10.1016/j.apcata.2005.06.008.